Quinolinic acid induces alterations in neuronal subcellular compartments, blocks autophagy flux and activates necroptosis and apoptosis in rat striatum.

Carlos Alfredo Silva-Islas
Instituto Nacional de Neurologia y Neurocirugia Manuel Velasco Suarez
Ricardo Alberto Santana-Martinez
Instituto Nacional de Neurologia y Neurocirugia Manuel Velasco Suarez
Juan Carlos León-Contreras
Instituto Nacional de Ciencias Medicas y Nutricion Salvador Zubiran
Diana Barrera-Oviedo
Universidad Nacional Autonoma de Mexico Facultad de Medicina
Jose Pedraza-Chaverri
Universidad Nacional Autonoma de Mexico Facultad de Quimica
Rogelio Hernandez-Pando
Instituto Nacional de Ciencias Medicas y Nutricion Salvador Zubiran
Perla Maldonado (maldonado.perla@quimica.unam.mx)
Instituto Nacional de Neurologia y Neurocirugia Manuel Velasco Suarez https://orcid.org/0000-0002-7629-0580

Research Article

Keywords: Quinolinic acid, excitotoxicity, autophagy impairment, necroptosis, apoptosis

Posted Date: March 24th, 2022

DOI: https://doi.org/10.21203/rs.3.rs-1443129/v1

Abstract

Quinolinic acid (QUIN) is an agonist of N-methyl-D-aspartate receptor (NMDAr) used to study excitotoxicity in animal models. Striatal QUIN administration increases intracellular Ca^{2+} and oxidative stress, induces cellular damage and activates different mechanisms of cellular death. There is evidence indicating that impairment in autophagy at early times contributes to cellular damage in excitotoxicity; however, the status of autophagy in QUIN model at 7 days remain unexplored. In this study, the ultrastructural analysis of subcellular compartments and the status of autophagy in the striatum of rats administered with QUIN (120 and 240 nmol) was performed at 7 days. QUIN induced motor behavior impairment, tissue neurodegeneration and cellular damage; moreover, promoted swollen mitochondrial crests, spherical-like morphology and mitochondrial fragmentation. QUIN decreased ribosomal density in the rough endoplasmic reticulum and myelin sheaths discontinuity in axons with separation of the compact lamellae. Furthermore, QUIN induced increase and decrease in ULK1 and p-70-S6K phosphorylation, respectively, suggesting autophagy activation; however, the increased microtubule-associated protein 1A/1B-light chain 3-II (LC3-II) and sequestosome-1/p62 (SQSTM1/p62), and decreased in Beclin 1 and mature cathepsin D also indicates a blockage in autophagy flux. Additionally, QUIN administration increased tumor necrosis factor alpha (TNFα) and receptor-interacting protein kinase 3 (RIPK3) as well as decreased B-cell lymphoma 2 (Bcl-2) and increased in Bcl-2-associated X protein (Bax) levels and c-Jun N-terminal kinase (JNK) phosphorylation, suggesting an activation of necroptosis and apoptosis, respectively. These results indicate that QUIN caused subcellular compartments alteration, a blockage autophagy flux and activated necroptosis and apoptosis at 7 days.

Introduction

Excitotoxicity is a common event in the physiopathology of a variety of neurological disorders like Alzheimer, Parkinson and Huntington diseases [1, 2]. This event involves overactivation of N-methyl-D aspartate (NMDA) receptors by agonists such as glutamate, NMDA and quinolinic acid (QUIN), increasing intracellular flux of Ca^{2+} from extracellular space, resulting in an imbalance in Ca^{2+} homeostasis. This imbalance triggers energetic depletion, activates different enzymes involved in reactive oxygen species (ROS) production, inducing an oxidative stress state in the cells, and activates proteases, lipases and endonucleases, leading to damage and cellular death [1, 3]. Moreover, there is increasing evidence supporting an alteration in autophagy pathway induced by excitotoxicity, which is associated with brain tissue damage [4, 5]; however, there is a great discrepancy about how this impairment causes tissue damage. The evidence supports an association of brain tissue damage and overactivation of autophagy [6], but also supports that a decrease in autophagy leads to brain tissue damage [5].

Macroautophagy is a degradation pathway of cellular components, where long-lived proteins and organelles are sequestered through the formation of a double-membrane (autophagosome) and then fused with lysosomes, forming an autolysosome, where the material is degraded [7].

The macroautophagy, hereafter autophagy, is a complex pathway that initiates with the formation of phagophore, induced by the activation of Unc51-like autophagy activating kinase 1 (ULK1) protein kinase complex, constituted by ULK1/2, autophagy related protein 13 (ATG13), focal adhesion kinase family interacting protein of 200 kDa (FIP200) and ATG101 proteins, and its translocation to the initiation sites, such as endoplasmic reticulum membrane [8]. Adenosine monophosphate (AMP)-activated protein kinase (AMPK) phosphorylates ULK1 protein in Ser^{317}, activating the ULK1 complex whereas mammalian target of rapamycin complex 1 (mTORC1) kinase phosphorylates to ULK1 in Ser^{757} inhibiting the ULK1 kinase complex [9]. The activated ULK1 complex recruits the class III phosphatidylinositol 3-kinase complex I (PI3KC3-C1) lipid kinase complex, integrated by vacuolar protein sorting 34 (VPS34), VPS15, Beclin 1, autophagy related protein 14-like (ATG14L), and nuclear receptor binding factor 2 (NRBF2) proteins, and phosphorylates the Ser^{15} on Beclin 1 and Ser^{249} on VPS34, activating the PI3KC3 complex, promoting the formation of phosphatidylinositol 3 phosphate (PtdIns3P), the recruitment of some proteins to the phagophore membrane [10] and the maturation of phagophore to autophagosome. Additionally, the sequestosome-1 SQSTM1/p62 (p62) protein, an autophagy receptor, binds to ubiquitinylated proteins and organelles that will be degraded by autophagy, and directs to the autophagosome through its interaction with microtubule-associated protein 1A/1B-light chain 3-II (LC3-II) protein, recruiting the material into the autophagosome [reviewed in 11]. Autophagosome binds to the lysosomes, which contain degradative proteases such as cathepsin D, an aspartic lysosomal protease, promoting protein degradation in autolysosomes [12].

Additional to the impairment in autophagy pathway due to excitotoxic process, there is evidence supporting the activation of necroptosis as a consequence of excitotoxicity, inducing cellular damage and neuronal death [13, 14]. Necroptosis is a regulated cellular death variant of necrosis that is activated by specific death receptors such as tumor necrosis factor receptor 1 (TNFR1), inducing assemble of necrosome, composed by proteins such as receptor-interacting protein kinase 1 (RIPK1) and receptor interacting protein kinase 3 (RIPK3). The binding of TNFR1 to tumor necrosis factor alpha (TNF-α), its ligand, promotes the auto-phosphorylation of RIPK1 that phosphorylates to RIPK3, which induces mixed lineage kinase domain-like protein (MLKL) phosphorylation. Phosphorylation of MLKL translocates it to cellular membrane forming a pore, inducing cell lysis and morphological characteristics of necrotic cell death. Necroptosis is observed in different neurological disorders like Alzheimer, Parkinson and cerebral ischemia [13, 15]. Furthermore, there is evidence indicating that necroptosis participates in axonal degeneration [13], neuronal death in excitotoxic models [14] and impairment in autophagy pathway, due to the translocation of MLKL to autolysosomal membranes, decreasing degradation [16].

QUIN is an active metabolite produced in the kynurenine pathway, the major route of tryptophan catabolism [17]. Under physiological conditions, QUIN is produced as an intermediate metabolite during the nicotinamide adenine dinucleotide (NAD^+) synthesis; however, as part of the neuroinflammatory processes, it is produced and released by infiltrating macrophages and activated microglia [18]. The extracellular presence of QUIN leads to an excessive activation of NMDA receptor inducing excitotoxicity [19], and an inhibition of glutamate uptake by astrocytes [20], extending the excitotoxic damage [21].

Striatal and intracerebroventricular administration of QUIN have been used as model for the study of the underlying mechanism of excitotoxicity in the striatum and hippocampus [22, 23].

There is evidence indicating than QUIN administration activates autophagy at early times (12 h after its administration) *in vivo* [24]. In contrast, when QUIN was incubated by 24 h *in vitro*, in primary neuron and astrocyte culture, the expression of Beclin 1 decreases and that of cathepsin D increases [12], suggesting inhibition [5] and activation [25] of autophagy at the same time. However, at 7 days, the role of QUIN on autophagy and the contribution of impaired autophagy to brain tissue damage remains unexplored. Additionally, to the impairment of autophagy due to QUIN administration at early times, there is evidence indicating that QUIN induces other types of cellular death such as apoptosis and necrosis. Morphological analyses *in vivo* suggest that QUIN induces a rapid cytoplasmic disintegration, characteristic of death by necrosis in the lesion core [26], but apoptotic cells are observed in areas surrounding the lesion core [27]. However, other types of cellular death such as necroptosis in brain tissue, after QUIN administration are still poorly studied. In this study we explore the effect of QUIN on morphological alterations in subcellular compartments, on the autophagy flux and necroptosis and apoptosis activation at 7 days in the rat striatum to determine if these pathways are involved in a secondary damage generating by QUIN administration.

Materials And Methods

Animals

Forty-five male Wistar rats (280-320 g) from the bioterium of Faculty of Medicine of the National Autonomous University of Mexico were kept under controlled conditions of temperature (25±3°C), humidity (50±10%), and lighting (12 h light/dark cycles). Animals had free access to standard commercial rat chow diet (Laboratory rodent diet 5001; PMI Feeds Inc., Richmond, IN, USA) and water *ad libitum*.

All procedures with animals were carried out strictly according to the National Institutes of Health Guide for the Care and Use of Laboratory Animals and to the Norma Oficial Mexicana NOM-062-ZOO-1999. The experimental procedures were approved by the Institutional and Local Committee for the Care and Use of Laboratory Animals on the Ethical Use of Animals from Instituto Nacional de Neurología y Neurocirugía Manuel Velasco Suárez, INNN project 44/15. During the experiments, all efforts were made to minimize animal suffering.

Reagents

QUIN, apomorphine, paraformaldehyde (PAF), glutaraldehyde, osmium tetroxide, sodium cacodylate, lead citrate, uranyl acetate, acrylamide, bis-acrylamide, ammonium persulfate, glycine, sodium dodecyl sulfate, phenylmethylsulfonyl fluoride (PMSF), pepstatin A, aprotinin, leupeptin, Triton® X-100, Folin & Ciocalteu's reagent, bovine serum albumin (BSA), rabbit anti-p62 antibody (P0067) and mouse anti-α-tubulin antibody (T9026) were purchased from Sigma-Aldrich (St. Louis, MO, USA). Rabbit anti-p62 (ab101266),

rabbit anti-RIP3 (RIPK3, ab56164) and rabbit anti-RIP3 (RIPK3, ab62344) antibodies were obtained from Abcam (Cambridge, MA, USA). Mouse anti-MAP LC3β (LC3-I/LC3-II, G-9; sc-376404), mouse anti-TNFα (52B83; sc-52746), mouse anti-RIP (RIPK1, C-12; sc-133102), mouse anti-BECN1 (Beclin 1, E-8; sc-48341) and mouse anti-cathepsin D (C-5; sc-377124) antibodies were obtained from Santa Cruz Biotechnology (Dallas, TX, USA). Rabbit anti-p-ULK1 Ser317 (12753), rabbit anti-ULK1 (8359), mouse anti-p-p70-S6K Thr389 (9206), rabbit anti-p70-S6K (9202), rabbit anti-p-JNK Thr183/Tyr185 (4671) and rabbit anti-JNK (9252) were obtained from Cell Signaling Technology (Danvers, MA, USA). Rabbit anti-Bax (GTX61026) was from Gene Tex (Irvine, CA, USA). Mouse anti-B-cell lymphoma 2 (Bcl-2, 14-6992) was from eBioscience Inc. (San Diego, CA, USA). Donkey-anti mouse IgG horseradish peroxidase-conjugate (715-035-150) and donkey-anti rabbit IgG horseradish peroxidase-conjugate (711-035-152) antibodies were from Jackson ImmunoResearch Laboratories Inc. (Jennersville, PA, USA). Fluoro-Jade B, polyvinylidene fluoride (PVDF) membrane, Immobilon Western kit and DPX mounting medium were obtained from Millipore (Bedford, MA, USA) and Universal L Kit SAB-System horseradish peroxidase (HRP) was from DAKO (Carpinteria, CA, USA). All the others reagents were obtained from known commercial sources.

Experimental design

Animals were randomly divided into three groups (n = 3-4) as follows: 1) SHAM group; 2) 120 nmol of QUIN (QUIN120); and 3) 240 nmol of QUIN (QUIN240). Animals from SHAM group received a unilateral striatal injection of isotonic saline solution (ISS) whereas the animals from QUIN120 and QUIN240 groups received a unilateral striatal injection of QUIN equivalent to 120 and 240 nmol, respectively. All animals were sacrificed at 7 days after ISS or QUIN administration and samples (striatum or perfused whole brain) were collected.

Four independent groups of animals were used for the evaluation of: 1) rotation behavior by apomorphine administration, neurodegeneration by Fluoro-Jade B staining and cellular and histological damage by hematoxylin and eosin (H&E) staining; 2) subcellular compartment alterations by transmission electron microscopy (TEM); 3) protein localization by immunohistochemistry; and 4) protein levels by Western blot (Fig 1).

Striatal administration

Rats were deeply anesthetized with sodium pentobarbital (40 mg/kg, *i.p.*), placed in a stereotaxic equipment (Stoelting Co., Woo Dale, IL, USA) and administered in the right striatum with 1 μL of ISS or QUIN (equivalent to 120 or 240 nmol) using a 10 μL Hamilton microsyringe (Hamilton Co., Reno, NV, USA). The administration was carried out according the following stereotaxic coordinates: +0.5 mm anterior to bregma, -2.6 mm lateral to bregma and -4.5 mm ventral to dura [28].

Rotation behavior

Six days after ISS or QUIN injection, animals were administered with apomorphine (1 mg/kg, *s.c.*) and placed in individual acrylic box cages. Five min later, the number of ipsilateral rotations was counted for 1 h. One rotation was defined as a complete 360º turn. Data were expressed as the total number of turns in 1 h.

Samples for histological analysis

Seven days after ISS or QUIN injection, animals were euthanized with sodium pentobarbital (100 mg/kg, *i.p.*) and perfused transcardially with ISS plus heparin (5 U/mL) followed by 4% PFA in 0.2 M phosphate buffer (pH 7.4). Brains were removed and post-fixed in 4% PFA for 48 h and subsequently dehydrated in ethanol and xylene solutions and embedded in Paraplast plus paraffin (McCormick Scientific, St Louis, MO, USA). Coronal sections of 5 µm were obtained in a HM 325 rotatory microtome (Thermo Fisher Scientific Inc., Waltham, MA, USA) every 100 µm, covering a total distance of 300 µm. These sections were used in Fluoro-Jade B, H&E and immunohistochemistry assays.

Fluoro-Jade B staining

Neurodegeneration was evaluated using Fluoro-Jade B staining. Sections were deparaffinized in xylene for 15 min and placed in absolute ethanol for 2 min, followed by 1% NaOH-80% ethanol solution for 5 min, 70% ethanol solution for 2 min and rinsed with distilled water for 2 min. Sections were immersed in 0.06% $KMNO_4$ solution for 10 min and rinsed with distilled water for 2 min. Finally, samples were stained with 0.0004% Fluoro-Jade B for 20 min, washed with distilled water, dried at 50ºC for 15 min, immersed in xylene and mounted with DPX mounting medium. Five fields in the striatum localized in areas surrounding the lesion core of the injection were counted with a Leica microscope (Cambridge, UK) using a 40X objective. Results were expressed as the number of positive cells to Fluoro-Jade B per field.

H&E staining

Cellular and histological damage was evaluated using H&E staining. Sections were deparaffinized in xylene and hydrated in solutions of decreasing ethanol concentration and distilled water. Sections were stained with hematoxylin for 1 min, then rinsed with distilled water and stained with eosin for 1 min. Finally, samples were dehydrated in solutions of increasing ethanol concentration and xylene, and mounted with DPX mounting medium. Five fields in the striatum localized in areas surrounding the lesion core of the injection were counted with a Leica microscope (Cambridge, UK) using a 40X objective. Results were expressed as the percent of damaged cells per field.

Immunohistochemistry

Histological localization of p62, MAP LC3 β (LC3), and RIPK3 was evaluated by immunohistochemistry. Sections were deparaffinized in xylene and hydrated in solutions of decreasing ethanol concentration and distilled water. Sections were permeabilized with phosphate buffered saline (PBS) plus 0.2% Triton® X-100 for 1 h, boiled in 10 mM sodium citrate buffer (pH 6.0) plus 0.2% Triton®

X-100 for 1 h and cooled at room temperature for 1 h. The peroxidase endogenous activity was inactivated with 1% hydrogen peroxide (H_2O_2) for 15 min. Sections were blocked with 2.5% BSA for 1 h at room temperature and then were incubated with rabbit anti-p62 (1:500; ab101266) antibody overnight and mouse anti-MAP LC3β (1:25) and rabbit anti-RIP3 (1:200; ab62344) antibodies during 48 h at room temperature. Sections were incubated with Universal L Kit SAB-System HRP according to the manufacturer's instructions. Finally, sections were incubated with 3,3'-diaminobenzidine, counterstained with hematoxylin and covered with DPX mounting medium. Sections in the striatum area were visualized in a Nikon E 200 microscope (Nikon, Melville, NY, USA) using 40X objective. Results were expressed as representative micrographs of each experimental group.

TEM

Subcellular compartment alterations were evaluated by TEM. Seven days after QUIN injection, rats (n=3 per group) were deeply anesthetized with pentobarbital (100 mg/kg, *i.p.*), and transcardially perfused with cool ISS followed by 4% PFA and 1.5% glutaraldehyde in Sörensen buffer (46 mM NaH_2PO_4, 154 mM Na_2HPO_4, 154 mM NaCl, pH 7.2). Brains were removed, the areas of interest dissected and fragmented, post-fixed in the same solution for 24 h, immersed in 1% osmium tetroxide in 0.1 M cacodylate buffer (pH = 7.2) and subsequently embedded in epoxy resin. Ultrathin sections (90 nm) of the striatal regions were obtained, contrasted with 3% lead citrate Reynolds and 1% uranyl acetate, and examined with a transmission electron microscope (FEI-Tecnai BioTWIN, Hillsboro, OR, USA). The ultrastructural analysis was carried out in neurons localized in the areas surrounding the lesion core of the injection.

Western blot

Protein levels of p-ULK1, ULK1, p-p70-S6K, p70-S6K, Beclin 1, preprocathepsin D, procathepsin D, cathepsin D, MAP LC3 β (LC3-I/LC3-II), p62, Bcl2, Bax, p-JNK, JNK, TNFα, RIPK1, RIPK3 were evaluated by Western blot. Seven days after ISS or QUIN administration, the right striatum of animals was collected and homogenized in 500 µL of cold lysis buffer (10 mM Tris HCl (pH 7.6), 15 mM NaCl, 0.25 mM sucrose, 1 µg/mL aprotinin, 1 µg/mL leupeptin, 1 µg/mL pepstatin A, 1 mM PMSF and 1% Triton® X-100) and centrifuged at 10,621 x g for 20 min at 4ºC. The supernatant was collected and the protein concentration was measured by Lowry method [29]. Fifty micrograms of supernatant were loaded in 10, 12 or 15% of polyacrylamide gel and proteins were separated and transferred to PVDF membranes. Membranes were blocked with 5% nonfat milk and incubated with primary mouse antibody anti-TNFα (1:500), mouse anti-RIP (1:500), rabbit anti-RIP3 (1:500; ab56164), mouse anti-BECN1 (1:500), mouse anti-cathepsin D (1:500), mouse anti-MAP LC3β (1:500), rabbit anti-p62 (1:1000; P0067), mouse anti-Bcl-2 (1:600), rabbit anti-Bax (1:600), rabbit anti-p-ULK1 (1:1000), rabbit anti-ULK1 (1:1000), mouse anti-p-p70-S6K (1:1000), rabbit anti-p70-S6K (1:1000), rabbit anti-p-JNK (1:1000), rabbit anti-JNK (1:1000) and mouse anti-□-tubulin (1:10000) overnight followed by the incubation of the secondary donkey antibody anti-mouse IgG horseradish peroxidase-conjugated (1:10000) or donkey antibody anti-rabbit IgG horseradish peroxidase-conjugated (1:10000). Membranes were revealed using an Immobilon Western kit (Millipore Co, Billerica, MA, USA) and images were obtained with a photodocumenter (Vilber Lourmat,

Eberhardzell, Deutschland). Images were analyzed using the ImageJ software (ImageJ v1.52a, NIH, Bethesda, MD, USA) and the data were expressed as relative optical density (OD) of the protein/β-tubulin.

Statistical analysis

All data are presented as the mean±SEM. Data were analyzed by one-way ANOVA and post hoc Tukey's test except for results of apoptosis that were analyzed by t-Student test using Prism 5.0 software (GraphPad, San Diego, CA, USA). Values of $P<0.05$ were considered to be statistically significant.

Results

QUIN induces rotation behavior impairment and brain tissue damage

QUIN is an endotoxin that induces excitotoxicity and increases oxidative stress, leading to tissue and cellular damage. QUIN120 tends to increase the number of ipsilateral turns per hour at day 6, however only QUIN240 increases significantly the number of ipsilateral turns compared to SHAM group (Fig. 2).

The impairment in rotation behavior in QUIN groups could be related with an increase in the neurodegeneration and tissue and cellular damage induced by QUIN at day 7. To explore this, we evaluated neurodegeneration and histological damage. SHAM group shows a mean of 4.06 positive cells per field to Fluoro-Jade B (Fig. 3a upper panel and 3b) and 23.23% of damaged cells (Fig. 3a, lower panel and 3c), that could be associated with the administration of ISS or the mechanical damage induced by the syringe during the striatal administration.

QUIN increases the number of cells in neurodegeneration (positive cells to Fluoro-Jade B) in a dose-response way with respect to SHAM group (Fig. 3a, upper panel). The number of positive cells to Fluoro-Jade B in QUIN120 and QUIN240 groups were 45.68 and 57.17, respectively (Fig. 3b). Besides, QUIN increases the percent of damaged cells per field in a dose-response way at 7 days (Fig. 3a, lower panel) to 68.84% and 86.56% in QUIN120 and QUIN240 groups, respectively (Fig. 3c). Furthermore, interstitial edema and the loss of neuropil integrity can be observed with the dose of 120 of QUIN, but is more evident in the QUIN240 group (Fig. 3a, lower panel).

QUIN induces damage in mitochondria and rough endoplasmic reticulum (RER)

We examined the effect of QUIN (120 and 240 nmol) on cellular organelles at 7 days post-lesion. Neurons from the SHAM group show well-preserved mitochondria, with intact crests (Fig. 4a and 4b). Nonetheless, in neurons of animals from the QUIN groups, the organelles are disorganized in the cytoplasm. QUIN120 produces neuronal swelling and dilatation of mitochondrial cristae compared to SHAM group (Fig. 4c and Fig. 4d). Moreover, QUIN240 increases the subcellular abnormalities compared with QUIN120 group; small and spherical-like morphology of mitochondria with extensive cristae dilatation are observed (Fig. 4e and 4f). Likewise, QUIN240 induces complete effacement of cristae and absence of intermembranal space of mitochondria with matrix effacement (Fig. 4f).

Otherwise, in the perinuclear cytoplasm of SHAM group, abundant well-developed RER and free ribosomes are observed (Fig. 5a and 5b), a characteristic consistent with its high protein synthesis activity. However, QUIN administration induces morphological alterations of RER in striatal neurons such as fragmentation and thinning of RER membrane, as well as a decrease of ribosomes (Fig. 5c-5f). Rats of QUIN120 group show fewer free ribosomes and lesser ribosomes in RER, as well as fragmented RER (Fig. 5c and 5d), and QUIN240 induces more accentuated subcellular abnormalities such as fragmented and thinner RER cisternae with scarce attached ribosomes (Fig. 5e and 5f).

QUIN induces axonal damage

We found that QUIN induces cellular damage as well as mitochondrial and RER damage, for that reason we evaluated the effect of QUIN on the axons of striatal neurons. In the SHAM group we observed intact axons with well-preserved myelin sheaths and axoplams some normal mitochondria and numerous microtubules (Fig. 6a, 6b and 6g).

QUIN induces alteration in the axon morphology and components, such as myelin layer discontinuity, separation of the compact myelin sheaths, and abundant fragmentation with disappearance of neurofilaments and microtubules. Rats of QUIN120 group show axon dilatation, neurofilaments disappearance, separation of myelin layer and disruption, producing vacuoles and total disruption (Fig. 6c and 6d) and QUIN240 produces even more axonal damage, many axons show thinner myelin layer and extensive disruption and fragmentation. Myelin layer exhibits extensive vacuolization and disruption (Fig. 6e and 6f).

QUIN blocks autophagy flux

There is evidence indicating that excitotoxicity impairs autophagy pathway and since we observed that QUIN induced mitochondrial damage, which could be associated to impairment in autophagy, we explore the status of autophagy flux. First, we performed an immunohistochemical analysis of p62 and LC3. In SHAM group, the detection of p62 and LC3 are low in striatal cells (Fig. 7). QUIN120 increases the cytoplasmic immunostaining of p62 and LC3 compared to SHAM group, Additionally, QUIN240 increased even more the staining of p62 and LC3. Interestingly, the positive labeling to p62 was commonly observed in the nucleus of neuronal cells in the three groups, particularly in the QUIN240 group. In both groups, QUIN120 and QUIN240, the immunostaining was more frequently in shrink neurons with pyknotic nuclei, and numerous swollen cells also showed strong immunostaining (Fig. 7).

The increase in p62 and LC3 levels could be an indicative in autophagy impairment, for that reason, we evaluated the autophagy pathway at different levels by western blot. Phosphorylation state of ULK1 in Ser^{317} and p-70-S6K in Thr^{389} was measured as indicative of activation of autophagy pathway. An increase in ULK1 phosphorylation and a decrease in p70-S6K phosphorylation levels in QUIN120 and QUIN240 groups was observed compared to SHAM group, suggesting an increase in autophagy (Fig. 8a and 8b). Surprisingly, Beclin 1 levels decrease after QUIN administration (120 and 240 nmol) compared with SHAM group (Fig. 8c). Moreover, p62 levels and in LC3-II/LC3-I ratio increase only in QUIN240 group

(Fig. 8d and 8e). Finally, the levels of procathepsin D were unchanged after QUIN treatment (Fig. 8f); however, a decrease in the maturation of cathepsin D was observed, since the levels of preprocathepsin D show a decrease in the QUIN240 group (Fig. 8g) and the levels of cathepsin D decrease with both doses of QUIN (Fig. 8h), suggesting a decrease in autophagy flux. These results suggest that QUIN240 (mainly), increases the activation of autophagy at early stages, but it promotes an autophagy flux blockage at late states on the pathway.

QUIN induces apoptosis

It has been reported, that the blockage in autophagy flux could be related to an increase in apoptosis or necroptosis [16, 30]. To explore the participation of apoptosis after QUIN treatment, we measured the levels of pro-apoptotic protein Bax, the anti-apoptotic protein Bcl-2, the Bax/Bcl-2 ratio and the activation (phosphorylation at Thr^{183}/Tyr^{185}) of JNK. QUIN240 decreases Bcl-2 levels and increases Bax levels, compared to SHAM group (Fig. 9a and 9b). Moreover, the Bax/Bcl-2 ratio (Fig. 9c) and the activation of JNK (Fig. 9d) increase in the QUIN240 group suggesting an activation of apoptosis pathway after 7 days. This was in agreement with the electron microscopy study that showed numerous nervous cells with condensed nucleus and almost preserved cytoplasm that correspond to apoptotic cells (Fig. 9e-g).

QUIN induces necroptosis

Also, in this work we explored the activation of necroptosis pathway as mechanism of tissue damage since alterations in axons and blockage in autophagy flux was observed after QUIN injection. The expression of RIPK3 protein, one of the principal indicators of necroptosis, was evaluated at 7 days. In SHAM group few cells showed slight immunostaining while QUIN treated group shower numerous positive cells (Fig. 10a). In QUIN120 group the main positive mark to RIPK3 is located in the cytoplasm and axons of shrink and swollen neurons. In QUIN240 group there are more RIPK3 immunostained in damaged nervous cells with cytoplasmic and nuclear immune-reactivity, endothelial cells also showed intense immunostaining (Fig. 10a).

The electron microscopy study confirms the extensive cellular damage and cell death, showing necrotic cells with pyknotic nucleus and shrinked cytoplasm or swollen neurons with chromatin disappearance and dilated cytoplasm with few and damaged organelles (Fig. 9f). The activation of the necroptotic pathway starts with the binding of TNFα to its cellular receptor, TNFR1, which promotes the phosphorylation of RIPK1, when caspase 8 is inhibited. This phosphorylation activates RIPK1 and induces the subsequent activation of RIPK3. To evaluate with more detail the necroptotic pathway, we measured the levels of TNFα, RIPK1 and RIPK3 by western blot, with the aim to support our finding in RIPK3 immunohistochemistry and determined whether necroptosis pathway could be participating in neuronal damage after QUIN administration. TNFα levels tend to increase in the QUIN120 group, but only QUIN240 increases TNFα levels compared to SHAM group (Fig. 10b). QUIN does not modify RIPK1 levels, nonetheless a tendency to increase is observed with QUIN240 (Fig. 10c). Finally, QUIN240 increases the

levels of RIPK3 compared to SHAM group, while QUIN120 only show a tendency to increase RIPK3 levels (Fig. 10d).

Discussion

Excitotoxicity is a common mechanism of cellular damage in neurological diseases and its study using molecules such as QUIN is an important tool for the description of different molecular events involved in cellular damage and death as well as in the search of potential therapeutic targets in these disorders. Excitotoxicity occurs when NMDA receptors are overactivated by agonist such as QUIN, inducing an increase in Ca^{2+} intracellular levels, promoting ROS production, and leading to cellular death [3].

In this work, QUIN caused impairment in rotation behavior of animals after apomorphine administration in a dose-response manner. Apomorphine is an agonist of dopamine receptors and its administration in animals with unilateral striatum lesion induces an ipsilateral rotation behavior, due to a decrease in dopamine receptor activity and the size of lesion is proportional to the speed of rotation [31]. The impairment in rotation behavior correlates with the extension of tissue damage, since QUIN increased neurodegeneration and cellular damage in a dose-response manner.

The cellular damage observed after QUIN administration (120 and 240 nmol) could be related with the increase in oxidative stress. Previous reports show that QUIN increases Ca^{2+} uptake from 30 min until 24 h after injection [32], generating an overproduction of hydroxyl radical and superoxide anion, at 50 min and 2 h, respectively [33, 34]. Also, the increase in ROS production induces lipoperoxidation at 2 h [35], decreases glutathione levels and increases the protein oxidation at 4 h after QUIN administration [36, 37]. Moreover, Colín-González et al. [37] reported that the inhibition of hemeoxygenase-1 exacerbates the damage induced by QUIN240 [37]. It has been reported that oxidative stress induced by QUIN causes damage in subcellular compartments such as mitochondria and RER in neurological diseases [38]. Here, QUIN induced in a dose-response way, dilatation of cristae and small and round mitochondrial morphology. These mitochondrial alterations could be a consequence of Ca^{2+} influx and/or by the overproduction of ROS, since mitochondria is involved in Ca^{2+} homeostasis and is the main source of ROS generation [39]. Also, as a consequence of the oxidative stress induced by QUIN, signaling pathways that promote cell death such as JNK pathway, could be activated at long times. Santana-Martínez et al. [40] reported an increase in p-JNK (active JNK) levels in mitochondria, which could be associated with apoptosis induction. Additionally, there are reports *in vivo* indicating that QUIN produces alterations in mitochondrial complexes [41], and mitochondrial dysfunction at 24 h [42] and 21 days post-lesion [41], which could be associated with the morphological alterations observed in mitochondria.

Additionally, in this work we observed alterations on RER morphology such as fragmentation and thinning membrane, as well as a decrease of ribosomes. The damaged observed in RER also follows a dose-response effect. Fernandes et al. [43] reported that QUIN decreases the sarco/ER Ca^{2+}-ATPase (SERCA)-mediated Ca^{2+} uptake in microsomal fractions of rat striatum, which could be involved in the

morphological alterations observed in RER with QUIN. Furthermore, damage in organelles and a decrease in ER were also observed in cells of rat liver in response to 60 nmol of QUIN [44].

QUIN also induced axonal damage in striatal neurons such as myelin sheaths discontinuity, separation of the compact myelin sheaths, and abundant fragmentation with disappearance of neurofilaments and microtubules. There is evidence indicating that QUIN is involved in demyelinating diseases, such as multiple sclerosis [45] and it is toxic to oligodendrocytes [46]. Moreover, the participation of excitotoxic processes has been observed in axonal damage. NMDA receptors in compact myelin of oligodendrocytes (part of oligodendrocyte that surrounds the axon cylinder of neurons) in optic nerve cells, induces accumulation of Ca^{2+} in myelin sheets during ischemia injury, leading to damage in the myelin sheath [47]. Additionally, the glutamate-induced excitotoxic process causes axonal degeneration through the activation of the necroptotic pathway [13].

There are reports indicating that excitotoxicity and oxidative stress promote disruption in autophagy flux and in consequence promote the accumulation of damaged organelles, increasing cell damage [5, 48]. Previously, the autophagy flux blockage was observed in excitotoxic models at early times in hippocampal neurons [4] and in the striatum of rats administered with glutamate [49]. The blockage in autophagy flux has been associated with the increase in cellular damage and cellular death [4]. In this work, we observe that QUIN240 increased the levels of p62 and LC3-II suggesting a blockage in autophagy flux, this proposal is supported by the reduction in mature cathepsin D and Beclin 1 levels, despite the increase observed in ULK1 phosphorylation and the decrease in p70-S6K phosphorylation.

The initiation of autophagy is regulated by the phosphorylation of ULK1 by mTORC1 and AMPK kinases. mTORC1 phosphorylates the Ser^{757} in ULK1 inhibiting the ULK1 complex, and decreasing the autophagy pathway; on the other hand, phosphorylation of Ser^{317} in ULK1 by AMPK activates the ULK1 complex activating the autophagy pathway [9]. The increase in Ser^{317} phosphorylation on ULK1 suggests an activation of autophagy; moreover, the decreases in Thr^{389} phosphorylation in p70-S6K, a target of mTORC1, support an activation of autophagy, since indicates a decrease in mTORC1 activity. These results suggest an increase in autophagy at early stages; however, we found a decrease in Beclin1 and accumulation of LC3-II and p62 proteins, suggesting an impairment of this pathway in later stages, possible at phagophore formation level or later step such as lysosomal dysfunction.

Beclin 1 is an important protein involved in the autophagy pathway, it is required in nucleation of phagophore, is part of the PI3KC3 complex and mediates the localization of some proteins important in phagophore formation [11]. Nguyen et al. [30] reported a decrease in Beclin 1 levels induced by its cleavage by calpain in an excitotoxic and oxidative stress dependent mechanisms, according with our results. Furthermore, Bieri et al. [50] reported a decrease in Beclin 1 by its cleavage induced by caspase 3 in patients with Alzheimer disease, hAAP transgenic mouse model and excitotoxic model-induced by kainic acid. The decrease of Beclin 1 inhibit the autophagy, but increase the cell damaged-induced by NMDA administration though excitotoxic process [5]. Excitotoxicity is involved in the cellular damage induced by QUIN [3, 32, 34] and the activation of calpain has been reported after excitotoxic event [51].

The decrease in Beclin 1 levels observed in this work could be associated with the activation of caspase 3, since we observed a decrease in Bcl-2 and an increase in Bax levels and Bax/Bcl-2 ratio, indicating an activation of apoptosis, which suggest the activation of caspase 3. Indeed, we observed many apoptotic cells in our ultrastructural study. Moreover, is important to note that the decrease in Beclin 1 was observed 5 days after kainic acid administration [50], similar to our model (7 days after QUIN injection).

Additionally, the blockage in autophagy flux by QUIN was evident by the accumulation of LC3-II and p62 levels, since these two proteins are degraded in lysosomes during autophagy. This blockage cold be associated with the decrease in mature cathepsin D levels, an aspartic lysosomal protease important in the maintaining of protein degradation by lysosomes or by the activation of necroptosis. Cathepsin D decreases after cerebral ischemia [25, 52] and this decrease promotes lysosomal dysfunction, inducing blockage of autophagy flux, without altering the autophagy initiation [25]; furthermore, there is evidence indicating that knockout mice to cathepsin D presents accumulation of autophagosomes in neurons from brain cortex [53]. Moreover, the decrease of cathepsin D, compared with the decline in other cathepsins involved in lysosomal function such as cathepsin B and L, is the cause of autophagy dysfunction [25, 54] whereas the increase in cathepsin D levels in cerebral ischemia restore the autophagy flux and lead to neuroprotection against the damage in cerebral ischemia [25].

The decline in mature cathepsin D could be related to the decrease in its maturation process or increase in mature cathepsin D degradation, instead of impairment in its synthesis. We observed that QUIN240 does not alter the pre-cathepsin D levels, while decrease the maturation process, suggesting that the impairment in its synthesis does not occurs. According with our results, Hossain et al. [25] reported that decrease in cathepsin D levels after cerebral ischemia is not associated with decline in its synthesis.

The deficiency of cathepsin D is also associated with an increase in apoptosis in retinal photoreceptor cells [54]. Correlating with this report, we observed an increase in Bax levels and Bax/Bcl-2 ratio and decrease in Bcl-2 levels, as well as an increase in JNK phosphorylation suggesting an active apoptosis pathway, which could be associated with the decrease in mature cathepsin D as mentioned above. Moreover, evidence support that autophagy disruption promotes apoptosis activation [48].

Another possibility involved in blockage of autophagy flux is the lysosomal dysfunction promoted by activation of necroptosis pathway at early times. QUIN induces necrosis and apoptosis death in striatum [26, 27], however there is increasing evidence suggesting the participation of other types of cellular death such as necroptosis, since this pathway is observed in excitotoxic models [13, 14]. Necroptosis initiates with the signaling of TNFα to its receptor, inducing the activation of RIPK1 that activates RIPK3, and in consequence activates its late effector MLKL [55]. The necroptosis pathway is implied in brain damage after cerebral ischemia [55, 56], subarachnoid hemorrhage [57] and contributes to axonal degeneration in excitotoxic models [13]. Its activation occurs at early events in brain damage [57] followed by apoptosis induction [55], and the inhibition of necroptosis decrease cerebral damage [56, 58]. Despite the fact that necroptosis is an event that occurs early in brain damage with a major expression of RIPK3 between 24 to 48 h [55, 57], we observed an increase in RIPK3 and TNFα levels at 7 days after QUIN240, suggesting

that necroptosis remain active at this time. The levels of RIPK1 did not change compared to SHAM group, however a tendency to increase was observed in QUIN240 group, suggesting that at this time the activation of necroptosis decline. As mentioned above, the activation of necroptosis could be involved in the autophagy disruption observed in QUIN240 group, through to lysosomal dysfunction. Phosphorylated MLKL disrupt autolysosomal membrane, decreasing intralumninal lysosomal acidity, promoting autolysosomal dysfunction, and blocking the autophagy flux [16]. For that reason, the blocking in autophagy flux after QUIN administration could be associated to necroptosis activation at early times.

We propose that QUIN induced excitotoxicity and oxidative stress promoting cellular and subcellular compartment damage, which could be exacerbate by the blockage in autophagy flux, though the activation of necroptosis and apoptosis. Moreover, the axonal damage could be related with the activation of necroptosis (Fig. 11).

Conclusion

QUIN induces rotation behavior, neurodegeneration, and morphological alterations in mitochondria, RER and axons of striatal neurons at 7 days post-lesion, possibly through the impairment in autophagy and increase in necroptosis and apoptosis at early times.

Declarations

Funding

This work was supported by CONACYT [Grant No. A1-S-21433 to PDM].

Competing interest

The authors have no relevant financial or non-financial interest to disclose.

Author contribution

Conceptualization: Perla D. Maldonado, Carlos Alfredo Silva-Islas; Methodos: Carlos Alfredo Silva-Islas, Ricardo Alberto Santana-Martínez, Juan Carlos León-Contreras; Formal analysis and investigation: Carlos Alfredo Silva-Islas; Writing-original draft preparation: Carlos Alfredo Silva-Islas, Ricardo Alberto Santana-Martínez; Writing-review and editing: Carlos Alfredo Silva-Islas, Diana Barrera-Oviedo, Jose Pedraza-Chaverri, Rogelio Hernández-Pando, Perla D. Maldonado; Funding acquisition: Perla D. Maldonado; Resources: Perla D Maldonado; Supervision: Jose Pedraza-Chaverri, Rogelio Hernández-Pando, Perla D. Maldonado. All authors read and approved the final manuscript.

Data Availability

The datasets generated during and/or analysed during the current study are not publicly available due to we do not have a persistent link to datasets but are available from the corresponding author on

reasonable request.

Ethics approval

Not applicable.

Consent to participate

Not applicable.

Consent for publication

Not applicable.

Acknowledgements

Not applicable.

Disclosure of potential conflicts of interest

The authors of this manuscript declare that there are no potential conflicts of interest.

Research involving Human Participants and/or Animals

This research only involves animals. All procedures with animals were carried out strictly according to the National Institutes of Health Guide for the Care and Use of Laboratory Animals and to the Norma Oficial Mexicana NOM-062-ZOO-1999. The experimental procedures were approved by the Institutional and Local Committee for the Care and Use of Laboratory Animals on the Ethical Use of Animals from Instituto Nacional de Neurología y Neurocirugía Manuel Velasco Suárez, INNN project 44/15. During the experiments, all efforts were made to minimize animal suffering.

Informed consent

Not applicable.

References

[1] Dong XX, Wang Y, Qin ZH (2009) Molecular mechanisms of excitotoxicity and their relevance to pathogenesis of neurodegenerative diseases. Acta Pharmacol Sin 30:379-387. https://doi.org/10.1038/aps.2009.24

[2] Lai TW, Zhang S, Wang YT (2014) Excitotoxicity and stroke: identifying novel targets for neuroprotection. Prog Neurobiol 115:157-188. https://doi.org/10.1016/j.pneurobio.2013.11.006

[3] Mehta A, Prabhakar M, Kumar P, Deshmukh R, Sharma PL (2013) Excitotoxicity: bridge to various triggers in neurodegenerative disorders. Eur J Pharmacol 698:6-18.

https://doi.org/10.1016/j.ejphar.2012.10.032

[4] Kulbe JR, Levy JMM, Coultrap SJ, Thorburn A, Bayer KU (2014) Excitotoxic glutamate insults block autophagy flux in hippocampal neurons. Brain Res 1542:12-19. https://doi.org/10.1016/j.brainres.2013.10.032

[5] Pérez-Carrión MD, Pérez-Martínez FC, Merino S, Sánchez-Verdú P, Martínez-Hernández J, Luján R, Ceña V (2012) Dendrimer-mediated siRNA delivery knocks down Beclin 1 and potentiates NMDA-mediated toxicity in rat cortical neurons. J Neurochem 120:259-268. https://doi.org/10.1111/j.1471-4159.2011.07556.x

[6] Yin WY, Ye Q, Huang HJ, Xia NG, Chen YY, Zhang Y, Qu QM (2016) Salidroside protects cortical neurons against glutamate-induced cytotoxicity by inhibiting autophagy. Mol Cell Biochem 419:53-64. https://doi.org/10.1007/s11010-016-2749-3

[7] Lippai M, Lőw P (2014) The role of selective adaptor p62 and ubiquitin-like proteins in autophagy. Biomed Res Int 2014:832704. https://doi.org/10.1155/2014/832704

[8] Zachari M, Ganley IG (2017) The mammalian ULK1 complex and autophagy initiation. Essays Biochem 61:585-596. https://doi.org/10.1042/EBC20170021

[9] Kim J, Kundu M, Viollet B, Guan KL (2011) AMPK and mTOR regulates the autophagy through direct phosphorylation of Ulk1. Nat Cell Biol 13:132-141. https://doi.org/10.1038/ncb2152

[10] Hurley JH, Young LN (2017) Mechanisms of autophagy initiation. Annu Rev Biochem 86:225-244. https://doi.org/10.1146/annurev-biochem-061516-044820

[11] Peker N, Gozuacik D (2020) Autophagy as a Cellular Stress Response Mechanisms in the Nervous System. J Mol Biol 432:2560-2588. https://doi.org/10.1016/j.jmb.2020.01.017

[12] Braidy N, Brew BJ, Inestrosa NC, Chung R, Sachdev P, Guillemin G.J (2014) Changes in Chathepsin D and Beclin-1 mRNA and protein expression by the excitoxin quinolinic acid in human astrocytes and neurons. Metab Brain Dis 29:873-883. https://doi.org/10.1007/s11011-014-9557-9

[13] Hernández DE, Salvadores NA, Moya-Alvarado G, Catalán RJ, Bronfman FC, Court FA (2018) Axonal degeneration induced by glutamate excitotoxicity es mediated by necroptosis. J Cell Sci 131:pii:jcs214684. https://doi.org/10.1242/jcs.214684

[14] Li Y, Yang X, Ma C, Qiao J, Zhang C (2008) Necroptosis contributes to the NMDA-induced excitotoxicity in rat's cultured cortical neurons. Neurosci Lett 447:120-123. https://doi.org/10.1016/j.neulet.2008.08.037

[15] Yuan J, Amin P, Ofengeim D (2019) Necroptosis and RIPK1-mediated neuroinflammation in CNS diseases. Nat Rev Neurosci 20:19-22. https://doi.org/10.1038/s41583-018-0093-1

[16] Frank D, Vaux DL, Murphy JM, Vince JE, Lindqvist LM (2019) Activated MLKL attenuates autophagy following its translocation to intracellular membranes. J Cell Sci 132:jcs220996. https://doi.org/10.1242/jcs.220996

[17] Moroni F (1999) Tryptophan metabolism and brain function: focus on kynurenine and other indole metabolites. Eur J Pharmacol 375:87-100. https://doi.org/10.1016/S0014-2999(99)00196-X

[18] Espey MG, Chernyshev ON, Reinhard JFJr, Namboodiri MA, Colton CA (1997) Activated human microglia produce the excitotoxin quinolinic acid. Neuroreport 8:431-434. https://doi.org/10.1097/00001756-199701200-00011

[19] Schwarcz R, Foster AC, French ED, Whetsell WOJr, Köhler C (1984) Excitotoxic models for neurodegenerative disorders. Life Sci 35:19-32. https://doi.org/10.1016/0024-3205(84)90148-6

[20] Tavares RG, Tasca CI, Santos CE, Wajner M, Souza DO, Dutra-Filho CS (2000) Quinolinic acid inhibits glutamate uptake into synaptic vesicles from rat brain. Neuroreport 11:249-253. https://doi.org/10.1097/00001756-200002070-00005

[21] Guillemin GJ (2012) Quinolinic acid, the inescapable neurotoxin. FEBS J 279:1356-1365. https://doi.org/10.1111/j.1742-4658.2012.08485.x

[22] Beal MF, Kowall NW, Swartz KJ, Ferrante RJ, Martin JB (1988) Systemic approaches to modifying quinolinic acid striatal lesions in rats. J Neurosci 8:3901-3908. https://doi.org/10.1523/JNEUROSCI.08-10-03901

[23] Ganzella M, Jardim FM, Boeck CR, Vendite D (2006) Time course of oxidative events in the hippocampus following intracerebroventricular infusion of quinolinic acid in mice. Neurosci Res 55:397-402. https://doi.org/10.1016/j.neures.2006.05.003

[24] Wang Y, Dong XX, Cao Y, Liang ZQ, Han R, Wu JC, Gu ZL, Qin ZH (2009) p53 induction contributes to excitotoxic neuronal death in rat striatum through apoptotic and autophagic mechanisms. Eur J Neurosci 30:2258-2270. https://doi.org/10.1111/j.1460-9568.2009.07025.x

[25] Hossain MI, Marcus JM, Lee JH, Garcia PL, Singh V, Shacka, JJ, Zhang, J., Gropen TI, Falany CN, Andrabi SA (2021) Restoration of CTSD (cathepsin D) and lysosomal function in stroke is neuroprotective. Autophagy 17:1330-1348. https://doi.org/10.1080/15548627.2020.1761219

[26] Portera-Cailliau C, Price DL, Martin LJ (1997) Non-NMDA and NMDA receptor-mediated excitotoxic neuronal deaths in adult brain are morphologically distinct: further evidence for an apoptosis-necrosis continuum. J Comp Neurol 378:88-104. https://doi.org/10.1002/(SICI)1096-9861(19970203)378:1<88::AID-CNE5>3.0.CO;2-G

[27] Feng Q, Ma Y, Mu S, Wu J, Chen S, Ouyang L, Lei W (2014) Specific reactions of different striatal neuron types in morphology induced by quinolinic acid in rats. PLoS One 9:e91512.

https://doi.org/10.1371/journal.pone.0091512

[28] Paxinos G, Watson C (1998) The rat brain in stereotaxic coordinates. Academic Press Inc San Diego: Press, USA.

[29] Lowry OH, Rosebrough NJ, Farr AL, Randall LJ (1951) Protein measurement with the Folin-phenol reagent. J Biol Chem 193:265-275. https://doi.org/10.1016/S0021-9258(19)52451-6

[30] Nguyen HQ, Zada S, Lai TH, Pham, TM, Hwang JS, Ahmed M, Kim DR (2019) Calpain-induced Beclin1 cleavage stimulates senescence-associated cell death in HT22 hippocampal cells under the oxidative stress conditions. Neurosci Lett 701:106-111. https://doi.org/10.1016/.neulet.2019.02.036

[31] Schwarcz R, Guidetti P, Sathyasaikumar KV, Muchowski PJ (2010) Of mice, rats and men: Revisiting the quinolinic acid hypothesis of Huntington's disease. Prog Neurobiol 90:230-245. http://doi.org/10.1016/j.pneurobio.2009.04.005

[32] Pierozan P, Fernandes DG, Dutra MF, Pandolfo P, Ferreira F, de Lima BO, Porciúncula L, Wajner M, Pessoa-Pureur R (2014) Biochemical, histopathological and behavioral alterations caused by intrastriatal administration of quinolic acid to young rats. FEBS J 281, 2061-2073. https://doi.org/10.1111/febs.12762

[33] Santamaría A, Jiménez-Capdeville ME, Camacho A, Rodríguez-Martínez E, Flores A, Galván-Arzate S (2001) In vivo hydroxyl radical formation after quinolinic acid infusion into rat corpus striatum. Neuroreport 12:2693-2696. https://doi.org/10.1097/00001756-200108280-00020

[34] Maldonado PD, Molina-Jijón E, Villeda-Hernández J, Galván-Arzate S, Santamaría A, Pedraza-Chaverrí J (2010) NAD(P)H oxidase contributes to neurotoxicity in an excitotoxic/prooxidant model of Huntington's disease in rats: protective role of apocynin. J Neurosci Res 88:620-629. https://doi.org/10.1002/jnr.22240

[35] Santamaría A, Rios C (1993) MK-801, an N-methyl-D-aspartate receptor antagonist, blocks quinolinic acid-induced lipid peroxidation in rat corpus striatum. Neurosci Lett 159:51-54. https://doi.org/10.1016/0304-3940(93)90796-n

[36] Cruz-Aguado R, Francis-Turner L, Díaz CM, Antúnez I (2000) Quinolinic acid lesion induces changes in rat striatal glutathione metabolism. Neurochem Int 37:53-60. https://doi.org/10.1016/s0197-0186(99)00165-5

[37] Colín-González AL, Orozco-Ibarra M, Chánez-Cárdenas ME, Rangel-López E, Santamaría A, Pedraza-Chaverri, J, Barrera-Oviedo D, Maldonado PD (2013) Heme oxigenase-1 (HO-1) upregulation delays morphological and oxidative stress damage induced in an excitotoxic/pro-oxidant model in the rat striatum. Neuroscience 231:91-101. https://doi.org/10.1016/j.neuroscience.2012.11.031

[38] Ferreiro E, Baldeiras I, Ferreira IL, Costa, RO, Rego AC, Pereira CF, Oliveira CR (2012) Mitochondrial-and endoplasmic reticulum-associated oxidative stress in Alzheimer's disease: from pathogenesis to biomarkers. Int J Cell Biol 2012:735206. https://doi.org/10.1155/2012/735206

[39] Zündorf G, Reiser G (2011) Calcium dysregulation and homeostasis of neural calcium in the molecular mechanisms of neurodegenerative diseases provide multiple targets for neuroprotection. Antioxid Redox Signal 17:1275-1288. https://doi.org/10.1089/ars.2010.3359

[40] Santana-Martínez RA, León-Contreras JC, Barrera-Oviedo D, Pedraza-Chaverri J, Hernández-Pando R, Maldonado PD (2018) Sustained activation of JNK induced by quinolinic acid alters the BDNF/TrkB axis in the rat striatum. Neuroscience 383:22-32. https://doi.org/10.1016/j.neuroscience.2018.04.034

[41] Mishra J, Kumar A (2014) Improvement of mitochondrial function by paliperidone attenuates quinolinic acid-induced behavioural and neurochemical alterations in rats: implications in Huntington's disease. Neurotox Res 26:363-381. https://doi.org/10.1007/s12640-014-9469-9

[42] Luis-García ER, Limón-Pacheco JH, Serrano-García N, Hernández-Pérez AD, Pedraza-Chaverri J, Orozco-Ibarra M (2017) Sulforaphane prevents quinolinic acid-induced mitochondrial dysfunction in rat striatum. J Biochem Mol Toxicol 31:e21837. https://doi.org/10.1002/jbt.21837

[43] Fernandes AM, Landeira-Fernandez AM, Souza-Santos P, Carvalho-Alves PC, Castilho RF (2008) Quinolinate-induced rat striatal excitotoxicity impairs endoplasmic reticulum Ca2+-ATPase function. Neurochem Res 33:1749-1758. https://doi.org/10.1007/s11064-008-9619-7

[44] Beskid M, Zamecka E, Dybkowska-Klos H, Jachimowicz J, Kocjasz W (1995) Effect of quinolinic acid administration on rat liver: ultrastructural investigation. Exp Toxicol Pathol 47:375-379. https://doi.org/10.1016/s0940-2993(11)80352-0

[45] Lim CK, Smythe GA, Stocker R, Brew BJ, Guillemin GJ (2007) Characterization of the kynurenine pathway in human oligodendrocytes. Int Congr Ser 1304:213-217. https://doi.org/10.1016/j.ics.2007.07.011

[46] Cammer W (2001) Oligodendrocyte killing by quinolinic acid in vitro. Brain Res 896:157-160. https://doi.org/10.1016/s0006-8994(01)02017-0

[47] Micu I, Jiang Q, Coderre E, Ridsdale A, Zhang L, Woulfe J, Yin X, Trapp BD, McRory JE, Rehak R, Zamponi GW, Wang W, Stys PK (2006) NMDA receptors mediate calcium accumulation in myelin during chemical ischaemia. Nature 439:988-992. https://doi.org/10.1038/nature04474

[48] Chung Y, Lee J, Jung S, Lee Y, Cho JW, Oh YJ (2018) Dysregulated autophagy contributes to caspase-dependent neuronal apoptosis. Cell Detah Dis 9:1189. https://doi.org/10.1038/s41419-018-1229-y

[49] Montiel T, Montes-Ortega LA, Flores-Yáñez S, Massieu L (2020) Treatment with the keto body D-beta-hydroxybutyrate attenuates autophagy activation by NMDA and reduces excitotoxic neuronal damage in

the rat striatum in vivo. Curr Pharm Des 26:1377-1387.
https://doi.org/10.2174/1381612826666200115103646

[50] Bieri G, Lucin KM, O'Brien CE, Zhang H, Villeda SA, Wyss-Cora, T (2018) Proteolytic cleavage of Beclin 1 exacerbates neurodegeneration. Mol Neurodegener 13:68. https://doi.org/10.1186/s13024-018-0302-4

[51] Guemez-Gamboa A, Estrada-Sánchez AM, Montiel T, Páramo B, Massieu L, Morán J (2011) Activation of NOX2 by the stimulation of inotropic and metabotropic glutamate receptors contributes to glutamate neurotoxicity in vivo through the production of reactive oxygen species and calpain activation. J Neuropathol Exp Neurol 70:1020-1035. https://doi.org/10.1097/NEN.0b013e3182358e4e

[52] Chen JH, Kuo HC, Lee KF, Tsai TH (2015) Global proteomic analysis of brain tissue in transient ischemia brain damage in rats. Int J Mol Sci 16:11873-11891. https://doi.org/10.3390/ijms160611873.

[53] Koike M, Nakanishi H, Saftig P, Ezaki J, Isahara K, Ohsawa Y, Schulz-Schaeffer W, Watanabe T, Waguri S, Kametaka S, Shibata M, Yamamoto K, Kominami E, Peters C, von Figura K, Uchiyama Y (2000) Cathepsin D deficiency induces lysosomal storage with ceroid lipofuscin in mouse CNS neurons. J Neurosci 20:6898-6906. https://doi.org/10.1523/JNEUROSCI.20-18-06898.2000.

[54] Koike M, Shibata M, Ohsawa Y, Nakanishi H, Koga T, Kametaka S, Waguri S, Momoi T, Kominami E, Peters C, von Figura K, Saftig P, Uchiyama Y (2003) Involvement of two different cell death pathways in retinal atrophy of cathepsin D-deficient mice. Mol Cell Neurosci 22:146-161.
https://doi.org/10.1016/s1044-7431(03)00035-6

[55] Naito MG, Xu D, Amin P, Lee J, Wang H, Li W, Kelliher M, Pasparakis M, Yuan J (2020) Sequential activation of necroptosis and apoptosis cooperates to mediate vascular and neural pathology in stroke. Proc Natl Acad Sci U S A 117:4959-4970. https://doi.org/10.1073/pnas.1916427117

[56] Deng XX, Li SS, Sun FY (2019) Necrostatin-1 prevents necroptosis in brain after ischemic stroke via inhibition of RIPK1-mediated RIPK3/MLKL signaling. Aging Dis 10:807-817.
https://doi.org/10.14336/AD.2018.0728

[57] Yuan S, Yu Z, Zhang Z, Zhang J, Zhang P, Li X, Li H, Shen H, Chen G (2019) RIP3 participates in early brain injury after experimental subarachnoid hemorrhage in rats by inducing necroptosis. Neurobiol Dis 129:144-158. https://doi.org/10.1016/j.nbd.2019.05.004

[58] Chen T, Pan H, Li J, Xu H, Jin H, Qian C, Yan F, Chen J, Wang C, Chen J, Wang L, Chen G (2018) Inhibition of RIPK3 attenuates early brain injury following subarachnoid hemorrhage: possibly through alleviation necroptosis. Biomed Pharmacother 107:563-570.
https://doi.org/10.1016/j.biopha.2018.08.056

Figures

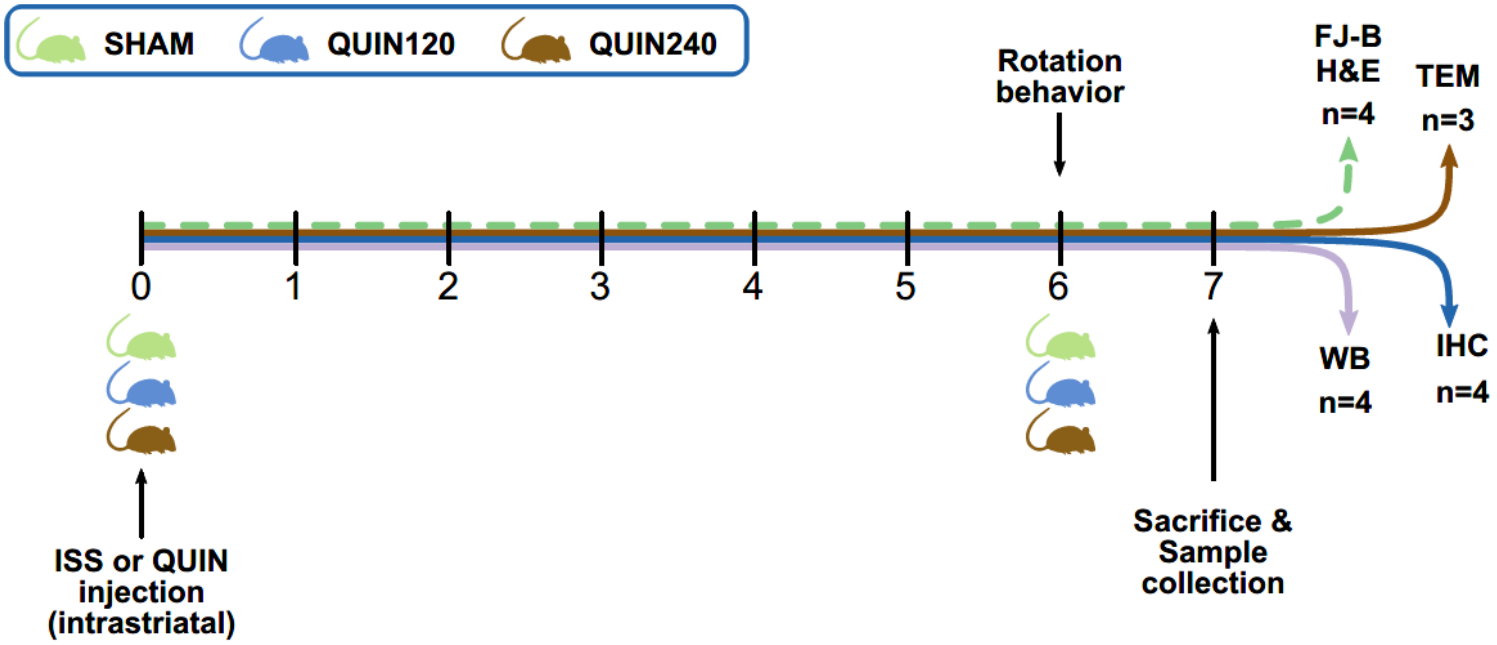

Figure 1

Experimental design. Rats were divided into three groups and administered in the right striatum with 1 µL of isotonic saline solution (ISS), SHAM group; or quinolinic acid 120 or 240 nmol, QUIN120 and QUIN240 groups, respectively. Rotation behavior was evaluated at day 6 after ISS or QUIN administration. Horizontal dotted arrow indicates the group of animals subjected to rotation behavior evaluation. Four independent groups of animals were sacrificed at day 7 after ISS or QUIN administration, as indicated with the four horizontal arrows in color, and the samples (striatum or perfused brain) were collected. The number of animals (n) used in each independent group is indicated. FJ-B: Fluoro-Jade B; H&E: hematoxylin and eosin; TEM: transmission electron microscopy; IHC: immunohistochemistry; WB: western blot (figure created with Inkscape 0.91)

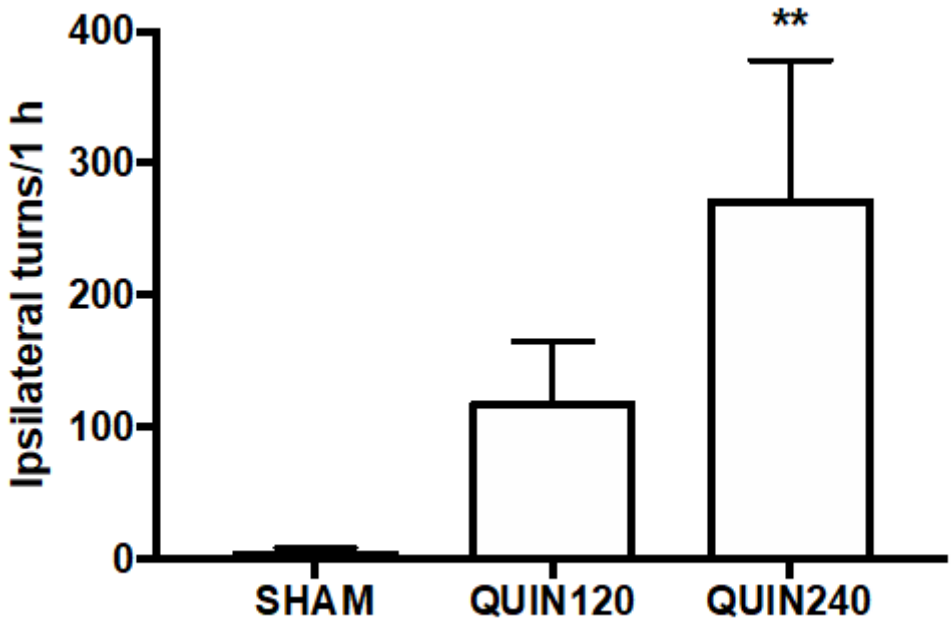

Figure 2

Rotation behavior induced by quinolinic acid (QUIN). Animals were administered in the right striatum with 1 µL of isotonic saline solution (SHAM group) or QUIN (120 or 240 nmol) and 6 days after were administered with apomorphine (1 mg/kg, *s.c.*). The number of ipsilateral turns were recorded for 1 h. Data are expressed as the mean ± SEM of four animals per group. **P<0.01 vs SHAM group

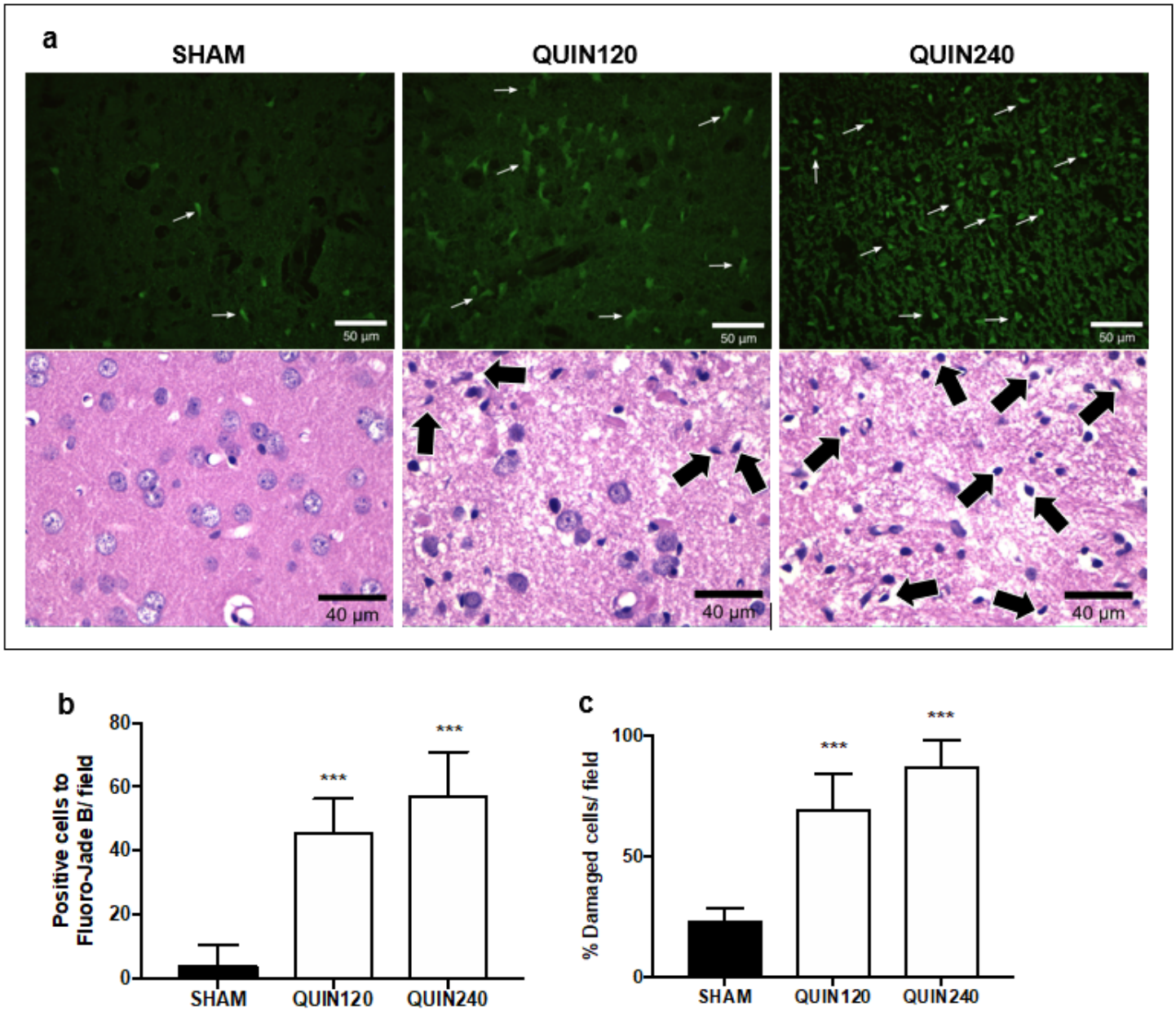

Figure 3

Histological striatal tissue damaged after quinolinic acid (QUIN) administration. Animals were administered in the right striatum with 1 µL of isotonic saline solution (SHAM group) or QUIN (120 or 240 nmol). Brains were collected and fixed after 7 days of the striatal injury, coronal sections (5 µm) were obtained and Fluoro-Jade B or hematoxylin and eosin (H&E) staining were performed. Representative micrographs (40x) of each group for Fluoro-Jade B staining (a, upper panel) and H&E staining (a, lower panel) are shown. White arrows show positive cells to Fluoro-Jade B (a, upper panel) and bold arrows show damaged cells (a, lower panel). b) The percentage of positive cells to Fluoro-Jade-B per field of three randomly fields (b) and the percent of damaged cells per field (c) in the striatum are presented in the graphs. Damaged neurons were identified by pyknotic nucleus and shrinking cytoplasm. Data are expressed as the mean ± SEM of four animals per group. ***P<0.001 vs SHAM group

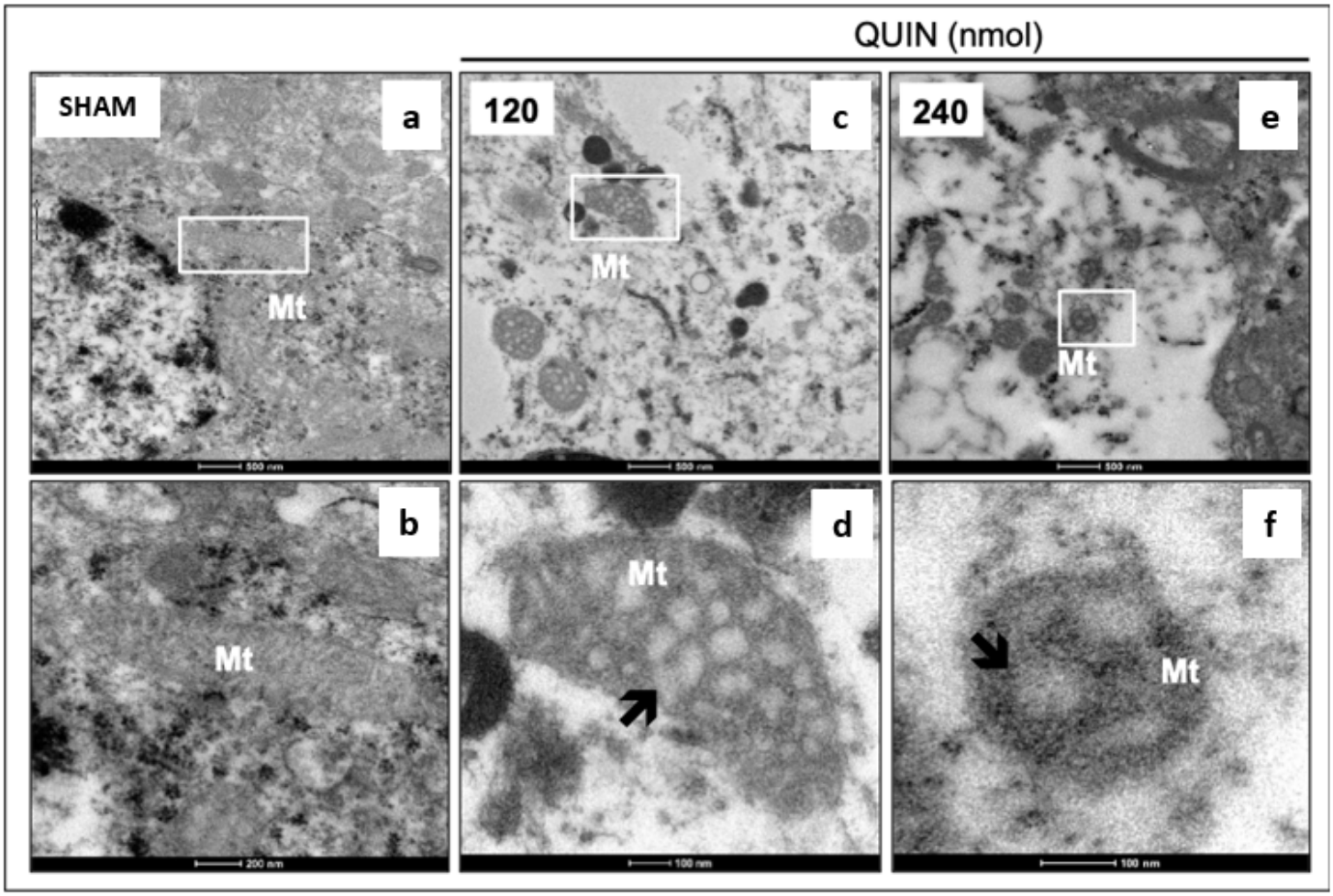

Figure 4

Mitochondrial alterations induced by quinolinic acid (QUIN) in striatal neurons of rat. Animals were administered in the right striatum with 1 µL of isotonic saline solution (SHAM group) or QUIN (120 or 240 nmol). Brains were collected and fixed 7 days after intrastriatal administration and transmission electron microscopy were performed. (a) Low power representative micrograph of normal neuron from SHAM group. (b) High power micrograph of mitochondria indicated in the inset of a with normal structure. (c) Cytoplasm of neuron from QUIN120 group shows wide dispersed and abnormal organelles. (d) High power micrograph from swollen mitochondria indicated in the inset of c shows dilated cristae. (e) Cytoplasm of neuron from QUIN240 group shows abnormal spherical mitochondria. (f) High power micrograph of spherical mitochondria circumscribed in the inset of e shows abnormal dilated cristae with effacement of the matrix. Bold arrows show dilatation of mitochondrial cristae. Mt = mitochondria

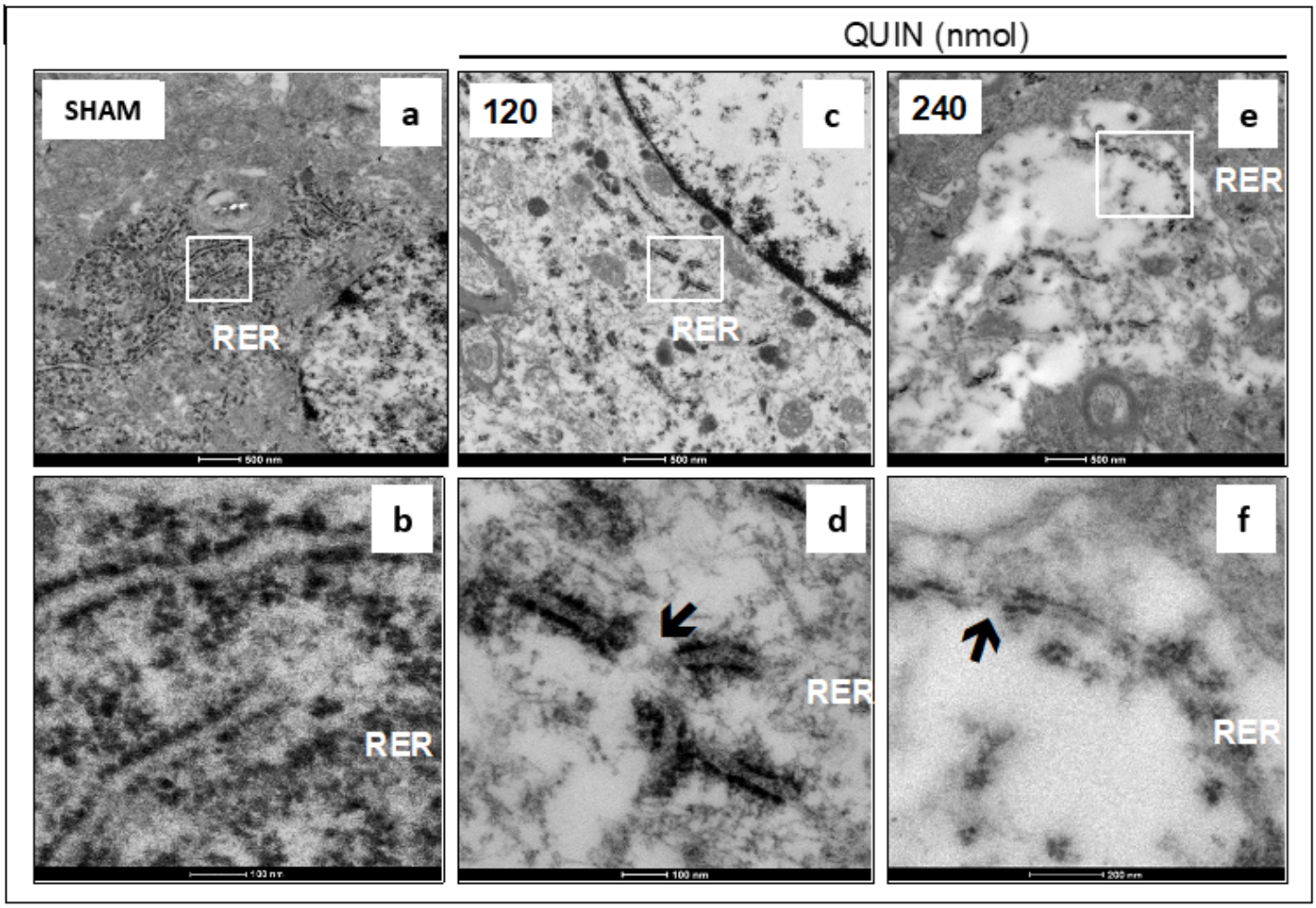

Figure 5

Rough endoplasmic reticulum (RER) alterations induced by quinolinic acid (QUIN) in striatal neurons of rat. Animals were administered in the right striatum with 1 µL of isotonic saline solution (SHAM group) or QUIN (120 or 240 nmol). Brains were collected and fixed 7 days after intrastriatal administration and transmission electron microscopy was performed. (a) Low power representative micrograph of normal neuron of SHAM group, with abundant and well developed RER. (b) High power micrograph of the inset area of a shows well-developed RER with numerous ribosomes. (c) Neuron from QUIN120 group show dispersed organelles with scare RER. (d) High power micrograph or RER indicated in the inset of c show fragmented RER (arrow) with almost complete disappearance of ribosomes. (e) Micrograph of neuron from group QUIN240 shows the cytoplasm with scare organelles. (f) High power micrograph of the inset in e shows RER constituted by thin and fragmented membranes (arrow) without ribosomes

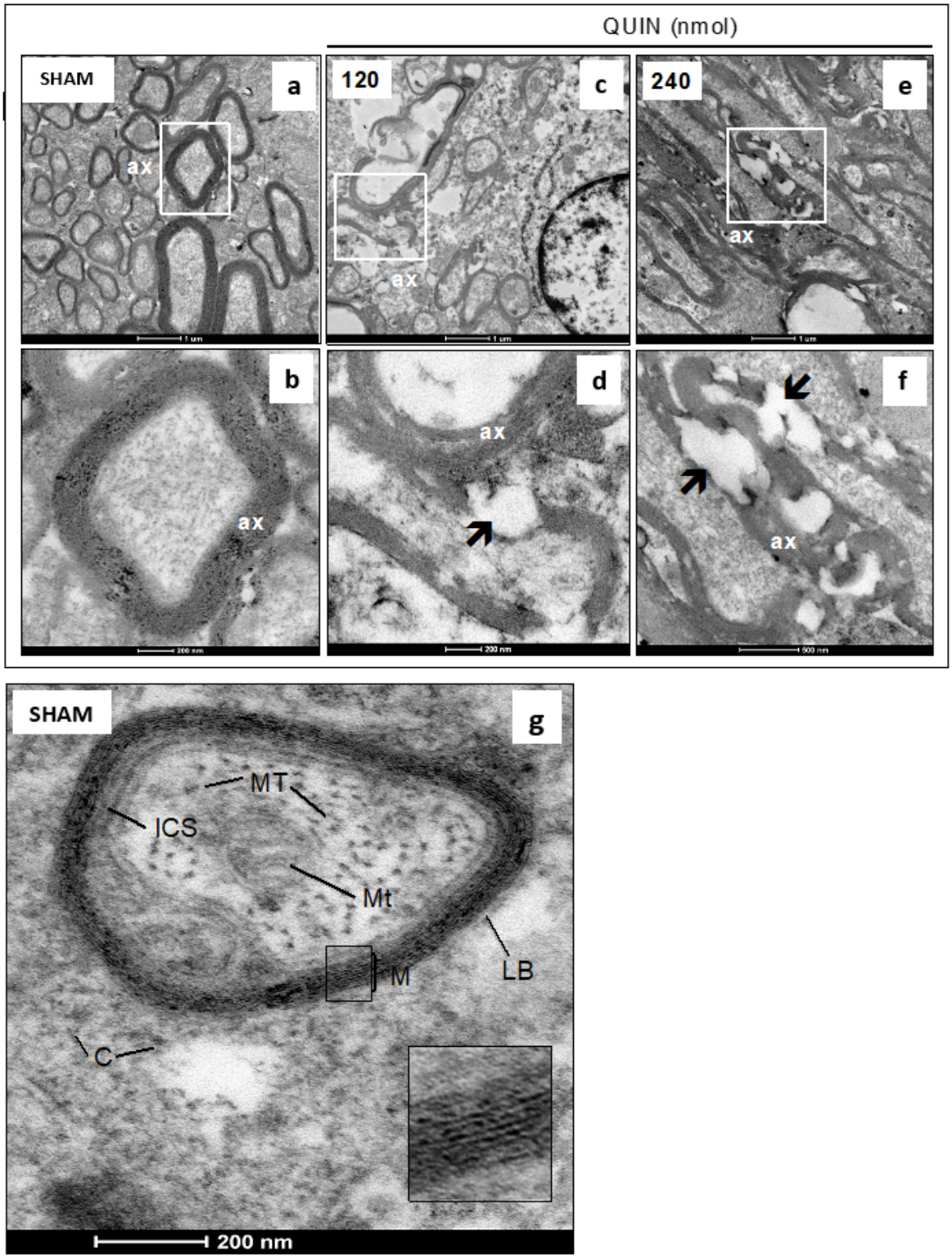

Figure 6

Axonal morphological alterations induced by quinolinic acid (QUIN) in striatal neurons of rat. Animals were administered in the right striatum with 1 µL of isotonic saline solution (SHAM group) or QUIN (120 or 240 nmol). Brains were collected and fixed 7 days after intrastriatal administration and transmission electron microscopy was performed. (a) Low power representative micrographs of axons (ax) of SHAM group. (b) High power micrograph on axon indicated by inset of a shows well-preserved myelin layer. (c)

Axon around a neuron from QUIN120 group, some of the, are swollen with disrupted myelin layer. (d) High power magnification of the inset of c that exhibit disruption of the myelin layer (arrow). (e) Striatal axons from QUIN240 group, come or them are thin with disrupted axon layer. (f) High magnification of the inset of e shows distention, vacuolization and extensive disruption (arrow) of the myelin layers. (g) Representative micrograph (200 nm) of axons from rats of SHAM group with numerous neurofilaments in transversal section, as well as mitochondria; in the inset is show the normal periodicity of the myelin layer (approximately 8-9 myelin sheaths). M, myelin sheaths; LB, basal lamina; Mt, mitochondria; MT, microtubules; ICS, internal collarette; C, collagen

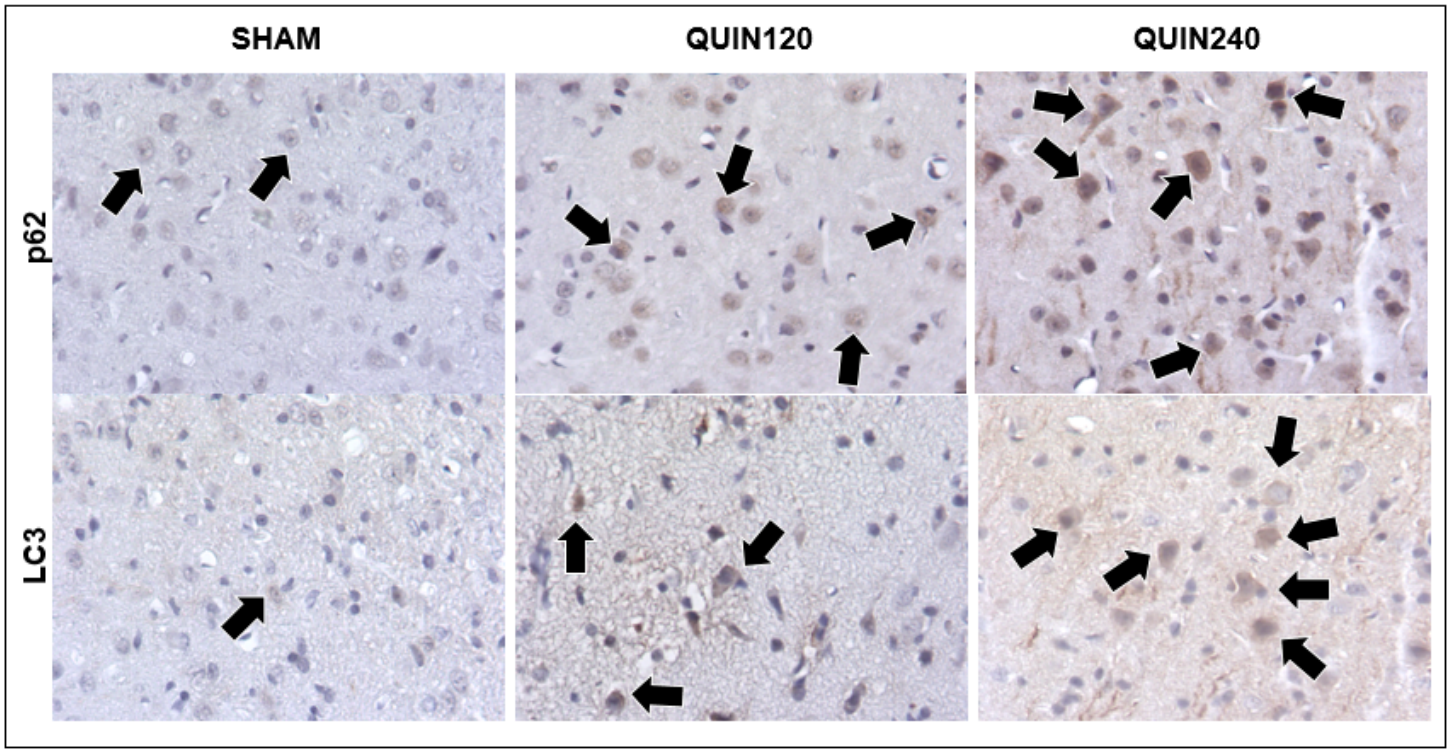

Figure 7

Effect of quinolinic acid (QUIN) on cellular localization of phosphotyrosine-independent ligand for the Lck SH2 domain of 62 kDa (p62) and microtubule-associated protein 1A/1B-light chain 3 (LC3) proteins by immunohistochemistry. Animals were administered in the right striatum with 1 µL of isotonic saline solution (SHAM group) or QUIN (120 or 240 nmol). Brains were collected and fixed 7 days after intrastriatal administration and immunohistochemistry were performed. Representative micrographs (40x) of the lesion core in the striatum of each group for p62 (upper panel) and LC3 (lower panel) are shown. Bold arrows show positive cells to p62 (upper panel) and LC3 (lower panel). Scare, almost negative p62 immunstaining is detected in sham group; in contrast, numerous neurons show p62 immunostaining in QUIN120 group, whereas the strongest p62 immunostaining is observed in swollen and shrinking neurons from QUIN240 group. Weak LC3 immunostaning is exhibited by striatal neurons

from sham group. Neurons from QUIN120 group show mild LC3 immunoreactivity and stronger LC3 immunostaining is exhibited by neurons in QUIN240 group

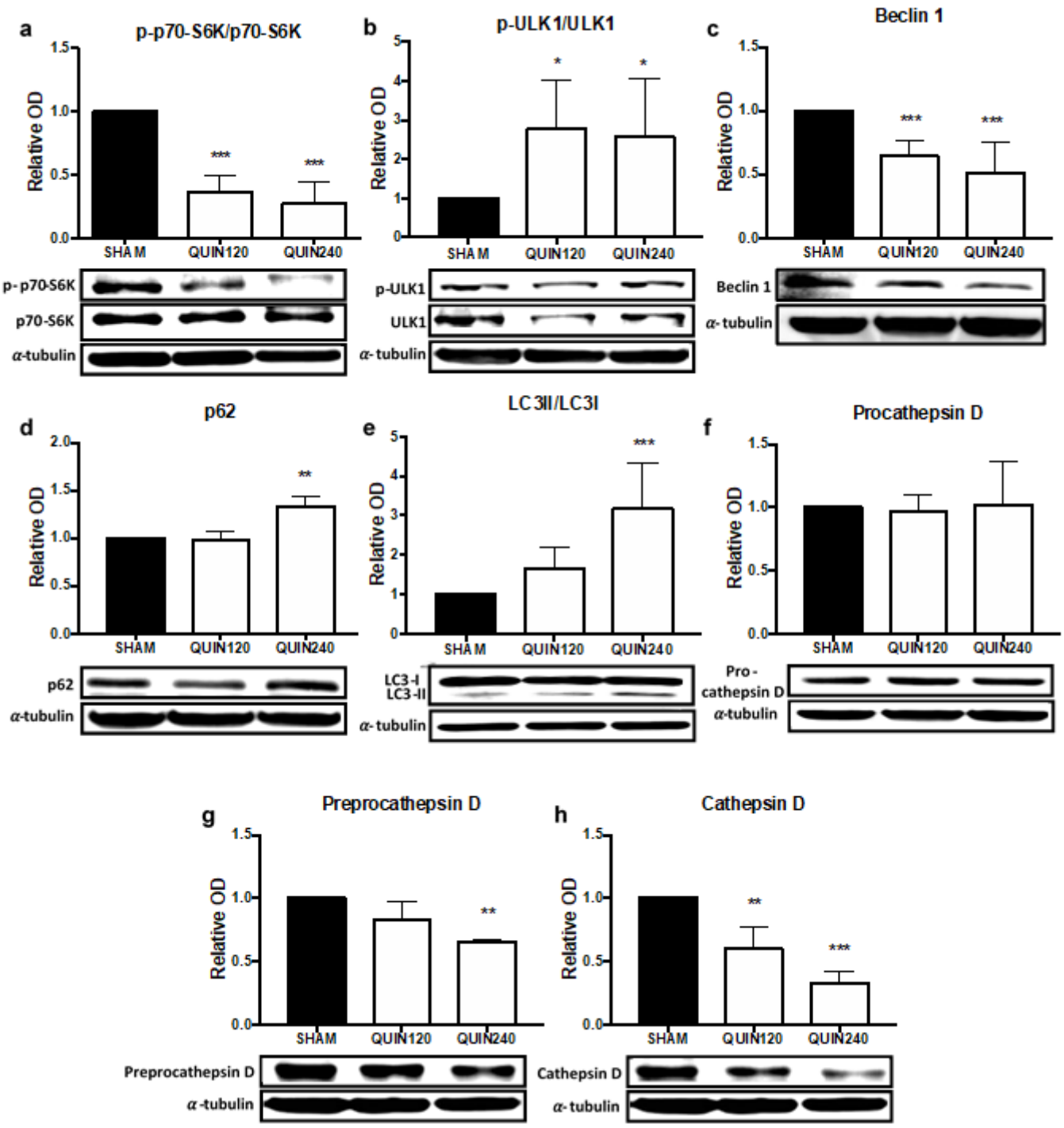

Figure 8

Effect of quinolinic acid (QUIN) on protein levels involved in autophagy pathway. Animals were administered in the right striatum with 1 µL of isotonic saline solution (SHAM group) or QUIN (120 or 240 nmol). Right striatums were collected at day 7 after intrastriatal administration and western blotting was

performed. Representative images of western blot and densitometric quantification of phosphorylated-ribosomal protein S6 kinase beta-1/ ribosomal protein S6 kinase beta-1 (p-p70-S6K(Thr389)/p70-S6K) ≈ 70 kDa/70 kDa (a), phosphorylated-Unc51-like autophagy activating kinase 1/ Unc51-like autophagy activating kinase 1 (pULK1(Ser317)/ULK1) ≈ 140 kDa/140 kDa (b), Beclin 1 ≈ 60 kDa (c), phosphotyrosine-independent ligand for the Lck SH2 domain of 62 kDa (p62) ≈ 62 kDa (d), microtubule-associated protein 1A/1B-light chain 3-II/I (LC3II/LC3I) ≈ 14k Da/16 kDa (e), procathepsin D ≈ 52 kDa (f), preprocathepsin D ≈ 46 kDa (g) and cathepsin D ≈ 34 kDa (h) are shown. Data are expressed as the mean ± SEM of four animals per group. *P<0.05, **P<0.01 and ***P<0.001 *vs* SHAM group. OD = Optical density

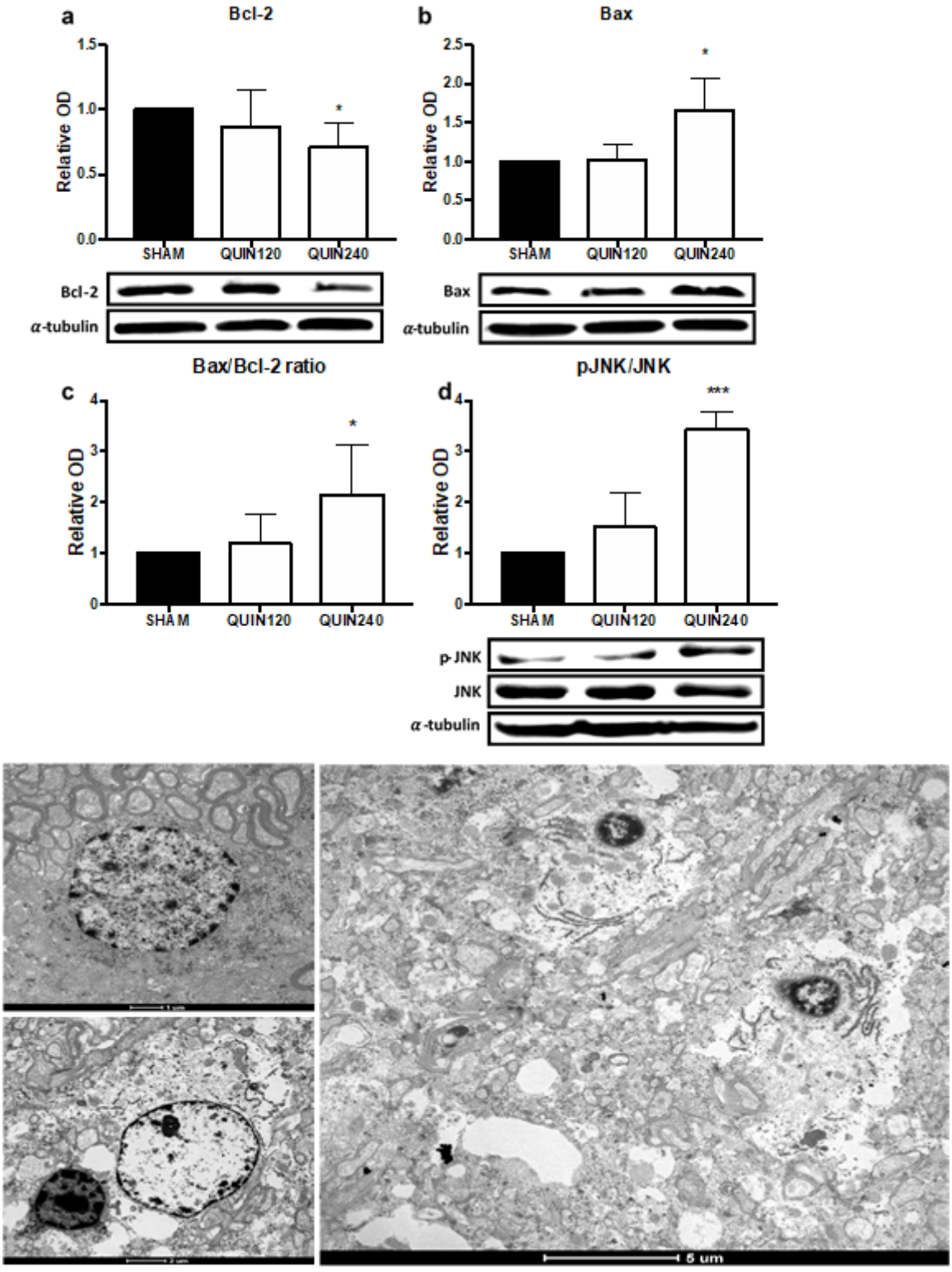

Figure 9

Effect of quinolinic acid (QUIN) on protein levels involved in apoptosis pathway. Animals were administered in the right striatum with 1 µL of isotonic saline solution (SHAM group) or QUIN (120 or 240 nmol). Right striatums were collected at day 7 after intrastriatal administration and western blotting was performed. Representative images of western blot and densitometric quantification of (a) B-cell lymphoma 2 (Bcl-2) ≈ 26 kDa, (b) Bcl-2-associated X protein (Bax) ≈ 20 kDa, (c) Bax/Bcl-2 ratio and (d)

phosphorylated-c-Jun N-terminal kinase/c-Jun N-terminal kinase (p-JNK (Thr183/Tyr185)/JNK) ≈ 54 kDa are shown. (e) Ultrastructure of normal neurons and axons from sham group. (f) The QUIN240 group exhibited shrinked (arrow) or swolled (asterisk) damaged neurons and (g) apoptotic neurons with condensed nucleus with relative preserved cytoplasm (arrows). Data are expressed as the mean ± SEM of four animals per group. *P<0.05 and ***P<0.001 *vs* SHAM group. OD = Optical density

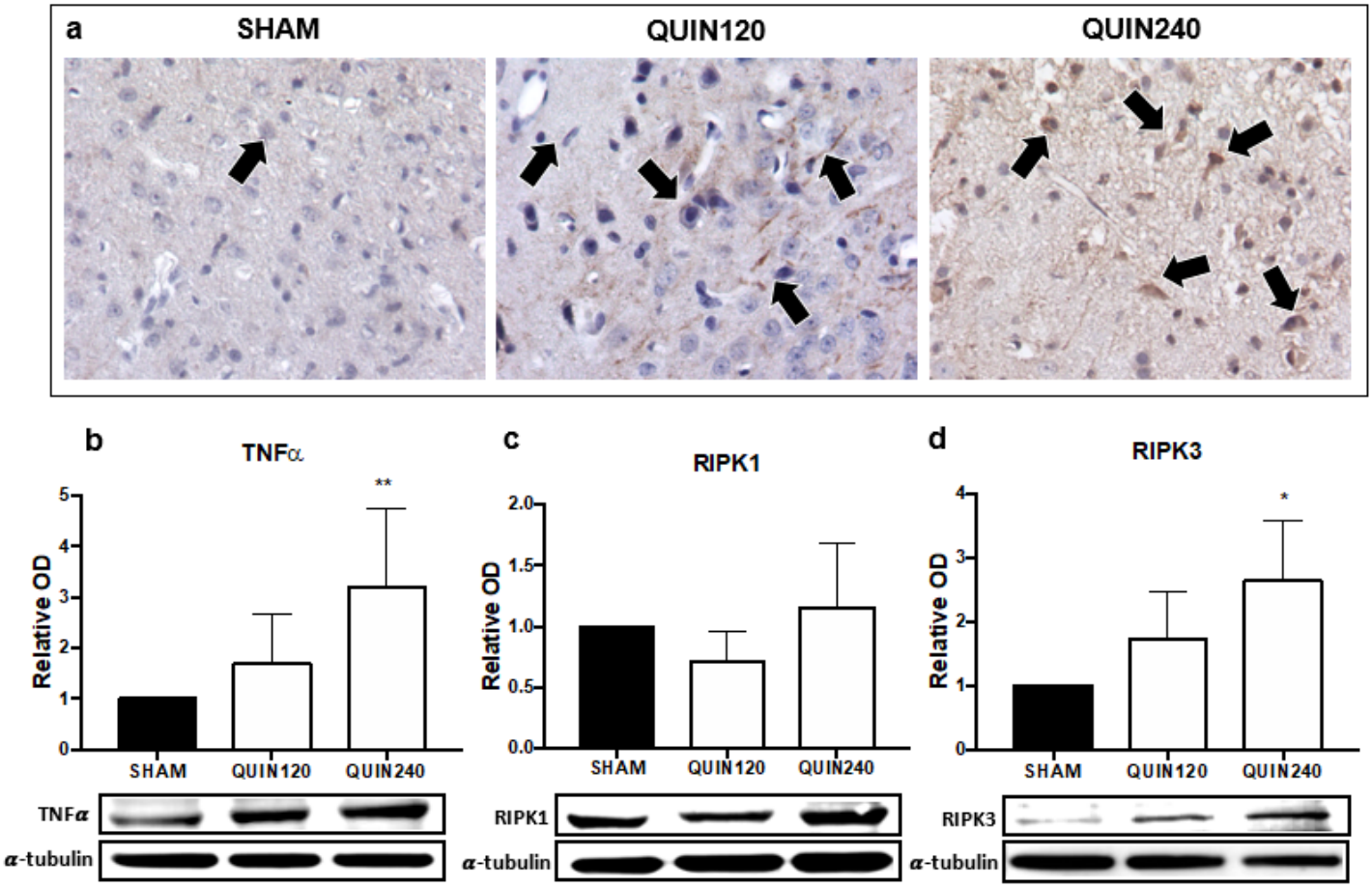

Figure 10

Effect of quinolinic acid (QUIN) on protein levels involved in necroptosis pathway. Animals were administered in the right striatum with 1 µL of isotonic saline solution (SHAM group) or QUIN (120 or 240 nmol). Brains for immunohistochemistry or right striatum for western blot were collected at day 7 after intrastriatal administration. (a) Representative micrograph (40x) of the lesion core of each group for receptor-interacting protein kinase 3 (RIPK3) are shown. Bold arrows show positive cells to RIPK3. Slight RIPK3 immunostaining is observed in striatal tissue from sham group; in comparison, neurons and axons from QUIN120 group shows mild RIPK3 immunoreactivity. Strong RIPK3 immunostaining is showed by damaged striatal neurons of QUIN240 group. Representative images of western blot and densitometric quantification of (b) tumor necrosis factor alpha (TNFα) ≈ 40 kDa, (c) receptor-interacting protein kinase

1 (RIPK1) ≈ 75 kDa and (d) RIPK3 ≈ 57 kDa are shown. Data are expressed as the mean ± SEM of four animals per group. *P<0.05 and **P<0.01 *vs* SHAM group. OD = Optical density

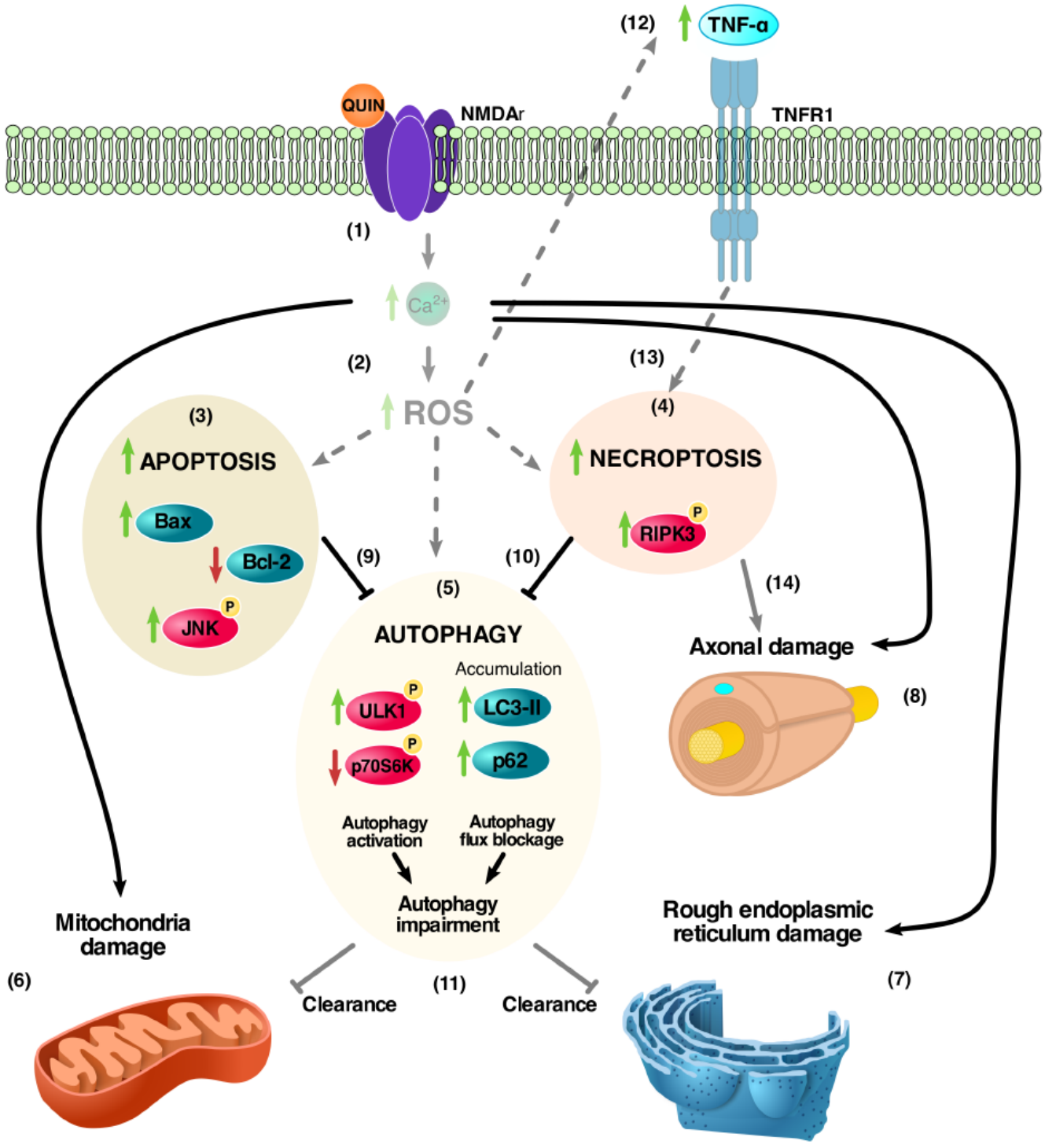

Figure 11

Effect of quinolinic acid (QUIN) on cellular damage in the striatum. Administration of QUIN in the striatum (1) promotes the increase of calcium in the cytoplasm of neurons through its binding to N-methyl-D-aspartate receptor (NMDAr), (2) increasing reactive oxygen species (ROS) levels. ROS could be responsible for the (3) apoptosis and (4) necroptosis activation and (5) autophagy impairment as well as damage to (6) mitochondria, (7) rough endoplasmic reticulum (RER) and (8) axon. At molecular level, QUIN increases (3) B-cell lymphoma 2 (Bcl-2)-associated X protein (Bax) protein levels and phosphorylation of c-Jun N-terminal kinase (JNK, activation) and decreases Bcl-2 protein levels, indicating activation of apoptosis pathway. Moreover, QUIN (4) increases the levels of receptor-interacting protein kinase 3 (RIPK3) suggesting necroptosis activation. Besides, (5) autophagy impairment occurs due to the autophagy activation by the increase in phosphorylation of Unc51-like autophagy activating kinase 1 (ULK1) at Ser^{317} and the inhibition of mammalian target of rapamycin complex 1 (mTOC1), evidenced by the decrease in phosphorylation of ribosomal protein S6 kinase beta-1 (p70S6K) at $Thr^{389,}$ as well as the blockage in autophagy flux, supporting by the accumulation of phosphotyrosine-independent ligand for the Lck SH2 domain of 62 kDa (p62) and microtubule-associated protein 1A/1B-light chain 3-II (LC3-II) proteins. This impairment in autophagy could be associated with (9) apoptosis and (10) necroptosis activation, since some proteins on these pathways interacts with autophagy proteins, dysregulating autophagy. (11) The impairment in autophagy could decrease the clearance of organelle damage, resulting in damaged mitochondria and RER accumulation in striatal cells. (12) Additionally, ROS could increase tumor necrosis factor alpha (TNF-α) levels promoting its binding to tumor necrosis factor receptor 1 (TNFR1), (13) activating the necroptosis pathway which (14) could contribute with axonal damage. The translucid elements and dotted arrows indicate possible mechanism associated with QUIN damage that in this work were not evaluated (figure created with Inkscape 0.91)